Study on formation of thin thermal stable titanium film on graphite for glass molding applications

Materials Technology- 4.semester

AALBORG UNIVERSITET

Jens Krarup

AALBORG UNIVERSITY
STUDENT REPORT

4th semester at the Department of Materials and Production
Master in Materials Technology
Fibigerstræde 16
9220 Aalborg Øst
http://www.mp.aau.dk

Title:

Study on formation of thin thermal stable titanium film on graphite for glass molding applications

Project:

Master Thesis

Project duration:

3rd February 2020 - 3rd June 2020

Author:

Jens Krarup

Supervisor:

Vladimir Popok

Number of pages: 56
Appendices: 4
Ended: 3-6-2020

Abstract:

In this project, an approach for developing thin thermal stable titanium film on graphite for glass molding applications was studied. Titanium films were deposited onto graphite substrates and subsequently annealed. The annealing led to film transformation from nanogranular to nanocrystallite phase which could be a rutile. The samples were put in contact with glass pieces under elevated temperatures to test their use in glass molding applications. Optical spectroscopy measurement showed no or very small reduction in transmittance of the glasses indicating no or negligible small sticking of the molds. The control sample (uncoated samples) caused a bit more significant decrease in transmission, indicating reaction with the glass. While the suggested approach on the coating of graphite molds with titanium seems to be successful, more studies on the optimization of film parameters are required.

Preface

This project is a master thesis submitted for the master-program Materials Technology at Aalborg University. This project is about the study of the formation of thin thermal stable titanium film on graphite for glass molding applications. There are no external partners involved in the project.

Readers guide The reference method used throughout this report is the Harvard-method. This means that the references will be mentioned as [Last name, Year], with the remaining information about the reference to be found in the bibliography. The books in the bibliography are listed as; title, author(s), year of release, ISBN-number along with the publisher and edition. Internet sites will be listed as; author(s), title, URL, release year and the day it was visited.

Contents

1 Introduction

Glass materials have become a key part of multiple consumer goods. Increasing consumer demands have lead to an increase in complexity in the final products. Examples are smaller aspherical lenses used in cellphone cameras, better optical components in the semiconductor industry for producing smaller microchips and the development of flat phone screens to fully 3d formed phone screens. Traditional methods of making lenses by grinding, polishing, and lapping are too time-consuming, expensive, and difficult to achieve with more advanced shapes [Zhang and Liu, 2017; Chao et al., 2013b]. Developed by the Eastman Kodak Company in the 1940s, Precision Glass Molding (PGM) has been proved to be an efficient manufacturing technique able to produce optical components rapidly. In essence, a glass ball is placed in the mold and heated to above its glass transition temperature (Tg) to ensure it can become more plastic and fill out the mold cavity, then when released from the cooled mold the glass will have the desired shape. The method has been traditionally used for optical components such as lenses, however, due to an increase in demand and the increased efficiency of PGM, the method is also used for 3D cover glasses for smartphones. The complexity of glass structures in smartphone architecture is likely to increase due to the advent of 5g smartphones [Chao et al., 2013a; Hong, 2017; Zhang et al., 2016].

The glass molding process occurs under high thermal and mechanical cyclic loads. As modern smartphone screens require the use of high Tg glass the thermal and mechanical load are further increased. Thus, the range of materials that can be used for glass molding is rather narrow.

A common material used to make molds is tungsten carbide, but it has the disadvantage of low machine-ability and a tendency to react upon contact with the glass.

Another material is that of fine grain graphite, which is easily machinable but is susceptible to oxidation at higher temperatures.

At high molding temperatures, the mold surfaces can react with the glass leading to glass sticking, thus, causing defects in the products and requiring the exchange of molds, strongly affecting the production cost.

Therefore, a thin protective coating is used to improve the lifetime of the molds.

The coating materials can be grouped into three categories: ceramics such as TiALN and CrN, amorphous carbon or diamond-like carbon and noble metal-based alloys. Out of these noble metal alloys are usually chosen for their chemical inertness and thereby anti-sticky properties. However, they do have a downside of having lower strength and high cost associated with them. Whereas ceramic coatings are widely used in different industries, and is a cheaper alternative. Yet, noble metal coatings outperform them at higher temperature [Ma et al., 2008; Klocke et al., 2010].

In a recent patent[Scoggins and Sheppard, 2019] (March 2019), a titanium-based coating is suggested for a graphite mold, which shows good results upon use with Gorilla Glas®.

Thus, this type of coating/mold system seems like a viable candidate to produce common consumer

goods such as smartphone screens. Yet, this type of coating is not well investigated and further research is warranted.

The goal of the project is to develop an approach on the formation of thin thermally stable titanium-based coatings on graphite to be used for glass molds. The research will include the study of structure and morphology of titanium films sputtered on graphite and the evolution of the film properties under thermal annealing.

2 Thin Film Coatings for Glass Molding

This chapter will cover the basics of the process of glass molding and cover in detail the usage of coating within the technology.

2.1 Glass molding

PGM is a thermal forming process that needs to be carried out in a controlled environment. A typical forming process includes distinct steps, that are illustrated in Figure 2.1 and 2.2.

The process cycle begins by placing a glass preform into the mold. The preform can be in the form of a ball, flat or near-net shape. Ball preforms are often used since they are cheap and are close to common lens shapes. Diverging from standard sizes such as large or very small preforms is a challenge. Flat preforms are easier to polished to high surface finish and are suited for molding micro/nano lens arrays and other thin components. They are also used for diverging lenses. Near-net shape preforms are used for complex geometry of larger dimensions. The production of near-net shape preform are costly.

Once the preform is placed in the mold, the chamber of the PGM machine is evacuated with an inert gas to ensure less sticking.

The first steps involve heating the mold and preform to the desired molding temperature which is above the T_g. There is no force applied to the system at this stage.

To ensure that the preform and mold have the same temperature, the temperature is held constant for some time. This is done because the temperature for the mold is the only thing that can be measured. This step is known as soaking, in some publications, this is included in the heating step.

Once the same temperature has been reached, the molding begins by applying force to mold and thereby deformation of the glass. Depending on the process, the parameters force, velocity, and position control are altered.

After reaching their final position, the molds are kept at lower force and a controlled cooling rate, this step is called annealing. This step is done until a temperature corresponding to the strain point of the glass is reached.

Lastly, the force is removed and the molds are separated and the lens and molds are cooled down. They are then removed from the machine and a new batch is prepared. [Zhang and Liu, 2017; Klocke et al., 2012].

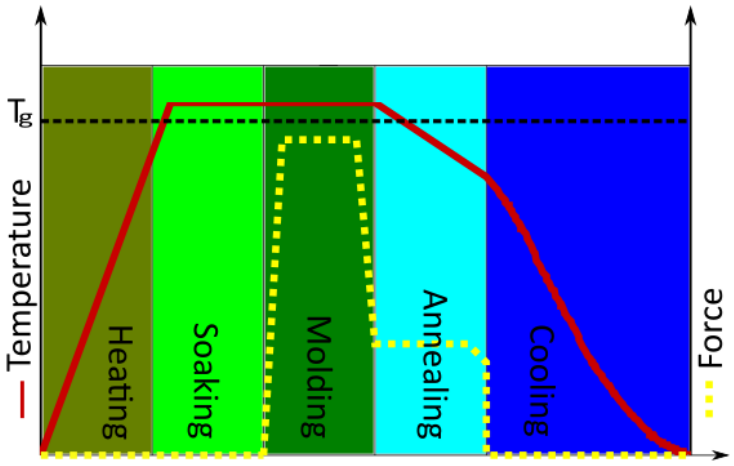

Figure 2.1: Main stages of a typical PGM process. The red curve indicates the temperature development during the process and the yellow curve represents the force development during the process.

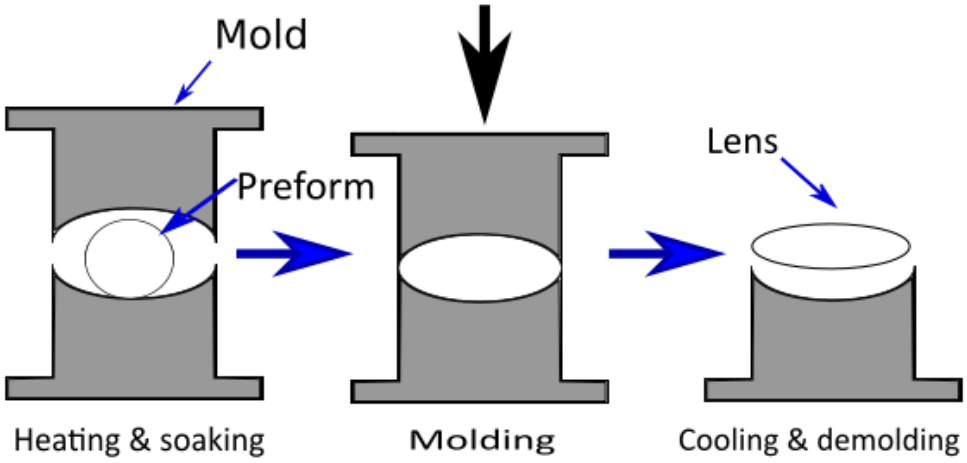

Figure 2.2: Schematics of a typical PGM process

It should be mentioned that this typical glass molding process (GMP) is known as an isothermal glass molding. Another method is the non-isothermal molding approach.

First, the glass preform is heated separately in a preheating unit. Then the high-temperature glass is moved to a molding unit where it is pressed together by the low-temperature molds. It is then annealed in the molds to ensure the release of internal stress. Lastly, the glass lens is now removed from the molds and moved to a cooling unit to return to room temperature.

This process has the advantage of a shorter cycle time as the next preform can be heated up while another is being molded, in addition, the temperature change of molds is smaller in comparison to the traditional method and thus, mold lifespan is improved. However, larger residual stresses are found in this process in comparison to the isothermal. Also, the setup is more advanced due to multiple units being required [Zang et al., 2014]. For both processes, only certain materials can handle the thermal and mechanical stress applied.

2.1.1 Mold material

The demands for a mold material as described in [Zhang and Liu, 2017] are the following: Excellent mechanical properties and wear resistance, a small coefficient of thermal expansion, outstanding thermal stability, and good machinability.

For so-called ultra-low Tg glass molding (process occurring below 400 °C) electroless nickel-phosphor is a commonly used material as it has high hardness, good wear resistance and corrosion resistance at moderate temperature. In addition, the material is cheap and has high machineability [Zhang and Liu, 2017]. However, above 400 °C properties begin to deteriorate due to crystallization. At higher temperature, a harder substrate is needed and thus, only a few particular materials such as tungsten carbide and silicon carbide can withstand the thermal and mechanical stress required. Some ceramics can also be used at higher temperatures. However, conventionally tungsten carbide is the material used [Zhang and Liu, 2017].

Tungsten carbide is chosen due to its stability and hardness even at elevated temperatures. The cons of using the material are the low machinability, due to its brittleness which increases cost as diamond grinding is the principal method used to form the molds [Chao et al., 2013a]. Lastly, due to interfacial reaction with the glass, the lifetime of the molds can be severely reduced [Zhu et al., 2015; Wei et al., 2019].

Another researched material is amorphous glass/carbon molds which in theory can work up to a temperature of 1500°C. However, research is inconclusive about its properties as investigation shows that oxidation-induced deterioration of properties and thermal mismatch problems can lead to instability in the mold [Maehara and Murakoshi, 2002; Liu et al., 2016].

Graphite can be also be used as a mold material. Graphite has the advantage of high machinability and good anti-sticky properties to glass. Yet it is susceptible to oxidation at higher temperatures. In addition, during machining pits can form on the mold [Scoggins and Sheppard, 2019].

Lastly per [Scoggins and Sheppard, 2019] the roughness margins are quite high for the graphite system (preferably deviations from average surface plane is less then 10µm) in question compared to other studies with tungsten carbide. Tungsten carbide is polished to have a surface roughness of less than 5 nm to be within the tolerance needed for optical products [Klocke et al., 2016; Peng et al., 2017]. Thus, if graphite is used as a molding material it should be used for a product with lower requirements such as phone screens.

For all mold types available high temperature can quickly cause wear and reaction with the glass. Therefore, to extend the lifetime of the mold and reduce cost a protective coating is used. [Zhang and Liu, 2017; Ma et al., 2008]

2.2 Coatings for glass molds

The primary function of coatings for glass molds is to extend the lifespan of the mold by providing a thermal and chemical barrier to avoid the most common failures; corrosion and glass sticking.

Within the glass molding industry, three main types of coatings are used: noble metal coatings, DLC, and ceramic coatings.

Several demands are applied to the coatings, they need to have adequate adhesion to the mold material, good thermal stability, and a similar coefficient of thermal expansion to match the mold to avoid cracking. In addition, the film needs to be able to have a good smooth surface and high hardness to ensure minimal loss of form accuracy. Protective films are also kept thin usually in the range of sub 1 µm to avoid cracks and to ensure the least amount of disturbance in the form accuracy. Thus, Physical Vapor Deposition (PVD) is utilized as a deposition method as this allows for better control with the composition, structure, and surface roughness of the coatings [Ma et al., 2008; Klocke et al., 2011; Chen et al., 2006].

In general, for all coatings and molds, it should be mentioned that the glass type used will have a large bearing on the performance of the coating for the specific task, as different coatings composition and/or combinations will work better in some situations than others [Chao et al., 2010, 2013b; Bobzin et al., 2014].

2.2.1 Noble metal coatings

Noble metal coatings have become the industry standard due to their relatively low chemical reactivity.

The relatively low chemical reactivity has become a more important property as glass manufactures have started to use network modifiers/additives which increases moldability. This can lead to an increased risk for failure during molding, as these additives can diffuse outwards onto the coating. Yet, even with increased moldability some types of glass still require high working temperature to be molded and there is still a strong need for coating with high hardness and strong oxidation resistance. Because despite the process occurring in a low oxygen atmosphere, it is still hard to avoid coating oxidation for some metal/alloys. [Liu et al., 2014; Tseng et al., 2011; Ma et al., 2008; Chao et al., 2013b]

A common noble metal coating system is PtIr, which fits well with the above requirements. Each metal individually has excellent corrosion resistance with iridium being the most corrosion-resistant metal known. Furthermore, it has the second-highest melting point of the platinum-group metal and one of the highest known modulus of elasticity. Iridium is commonly used to strengthen platinum elements and has a variety of uses in different industries Smith [2005].

However, both materials are not easy to fabricate into targets used for sputtering systems, and combined with the high price for raw material, the coast associated with this coating is its greatest

weakness.

The PtIr system is often used for tungsten carbide molds, however, to ensure proper adhesion an interlayer is needed, this is most commonly made using either Ni or Cr [Bobzin et al., 2010, 2012; Klocke et al., 2011].

However, the breakdown of the film is not only the result of chemical reaction with the glass but also due to diffusion from the mold and the adhesion layer.

Tungsten carbide is often sintered together with Co binders to improve mechanical properties. However, Co can diffuse outwards to the coating and start reacting with it causing cracks and reducing form accuracy.

Even without Co binders, the material from the adhesion layer can also diffuse into the coating causing intermetallic particles and voids to form. Ni tends to diffuse to the surface forming a metallic layer, while Cr forms oxides scales on top of the coating when diffused to the surface. The diffusion is strongly contributed to by the nanocrystalline columnar grain structure of the coating that enables short and fast diffusion pathways [Chao et al., 2013b; Klocke et al., 2016; Peng et al., 2017; Friedrichs et al., 2020].

A solution to this problem has been to use TaN as an adhesion layer. While it successfully creates a barrier layer it has the disadvantage of an even higher cost [Chien et al., 2010]

The Ir-Re system has been considered an interesting substitution. However, this system is also prohibitively expensive. Thus, alternatives have been sought after. Alternatives are usually Ru based refractive metal coatings such as Mo-Ru or Ta-Ru. While cheaper and showing some promising results this type of metal coatings is oxidized at around 600 °C and there is a need for further improvement before this type will be more efficient than the common Pt-Ir coatings [Chen et al., 2006; Liu et al., 2014; Chen et al., 2017].

2.2.2 Diamond-like coatings

DLC is a term that covers a wide array of carbon-based protective coatings. It is commonly used for its high wear resistance and as a friction protection layer for cutting tools, and other applications where low friction is needed.

It has been attempted to be utilized as a coating for GMP however, while studies suggested it could be a potential candidate, it tends to oxidize at higher working temperature and thus making it unfit for use of molding higher Tg glass.

Some positive results have been obtained where a higher sp^3 ratio has obtained by magnetron sputtering which improves properties. However, coating failure was still observed during annealing test at 650 °C.

It does have the advantage of being removable by etching process, making it easier to reuse the molds compared to other coatings. As e.g. noble metal coatings needs to be removed by

machining which requires re-machining to ensure proper form accuracy [Brand et al., 2004; Xie et al., 2011; Kim et al., 2007; Park and Won, 2010; Min et al., 2015; Bernhardt et al., 2013].

2.2.3 Ceramic coatings

Ceramic coatings are commonly used in a variety of industrial processes, especially for tools. They are characterized by high hardness and wear resistance.

In addition, they are resistant to thermal stress and thus, can be used for GMP. A disadvantage is the low oxidation resistance at elevated temperatures, which can lead to a large increase in surface roughness and reaction with glass surface resulting in glass sticking. Yet, the usage of ceramic-based coatings is highly sought after due to their low cost.

Ceramic coating comes in a wide range of different materials, a common feature is that they are often nitrides. Examples include: CrN, TaSIN, WCrN, and TiALN. While most of them exhibit good properties at lower working temperatures and, thus, are suitable for molding low Tg glass. However, noble metal coatings still tend to be superior at higher temperatures.

Also of interest for ceramic coatings is the composition as a large variety of them are ternary or higher-order alloys. Studies have shown that by precise control of the composition, the crystal structure of the coating can be change from crystalline to amorphous. Due to lack of grain boundaries, amorphous coatings can provide effective protection against oxidation of the substrate and thus, avoid the common failure methods that can be seen in e.g. the PtIr/Cr/WC system Suni et al. [1983]. It has also been suggested that the formation of oxide scales with an amorphous structure could provide protection for the coating [Chen and Wang, 2014].

Some studies highlighting the critical function of composition control during coating production are [Lee et al., 2018] and [Chen et al., 2015a]. In [Lee et al., 2018] AlCrN coating was produced and tested in a high-temperature environment. After annealing, it was seen that a distinctive area of the coating had pinholes and after further investigation, it was found that the area containing the pinholes had a different atomic ratio of Al/Cr then the rest of the coating. By using X-ray diffraction it could be seen that the area with pinholes contained oxides while the area without pinholes did not contain any oxides after annealing. Thus, due to the uneven formation of the coating, part of the coating was strongly oxidized.

In [Chen et al., 2015a] CrWN coating was produced by PVD. Several different compositions were made by varying sputtering power for the W and Cr targets and altering the Nitrogen flow. After mechanical testing four compositions were annealed in a low oxygen atmosphere. Here it was observed that the composition had a great impact on oxide formation. The higher Cr containing composition had either no apparent oxide formation or a small, but amorphous oxide formation thus, both retain high hardness and low surface roughness. In contrast compositions with lower Cr content had both thicker oxides and a severe decrease in hardness and a large increase in surface roughness. In a normal atmosphere, all coatings regardless of composition had thick oxide formation and a large increase in roughness and a drop in hardness. Furthermore, in [Chang et al.,

2017] by the same authors, other compositions were found to match the oxidation resistance but with better mechanical properties.

Thus, it can be seen that composition has a large effect on the performance of the coating.

Ceramic films in general have issues with oxide formation as this can lead to scale formation and thus increased roughness which strongly limits form accuracy and thus, making them unsuitable for lens production. An illustration of the concept using examples i.e. Scanning Electron Microscpy (SEM) images from [Chen et al., 2015a] where the high Cr content $Cr_{37}W_{31}N_{32}$ composition sees no oxide formation where as the low Cr content $Cr_8W_{69}N_{23}$ forms a thick oxide can be seen in Figure 2.3.

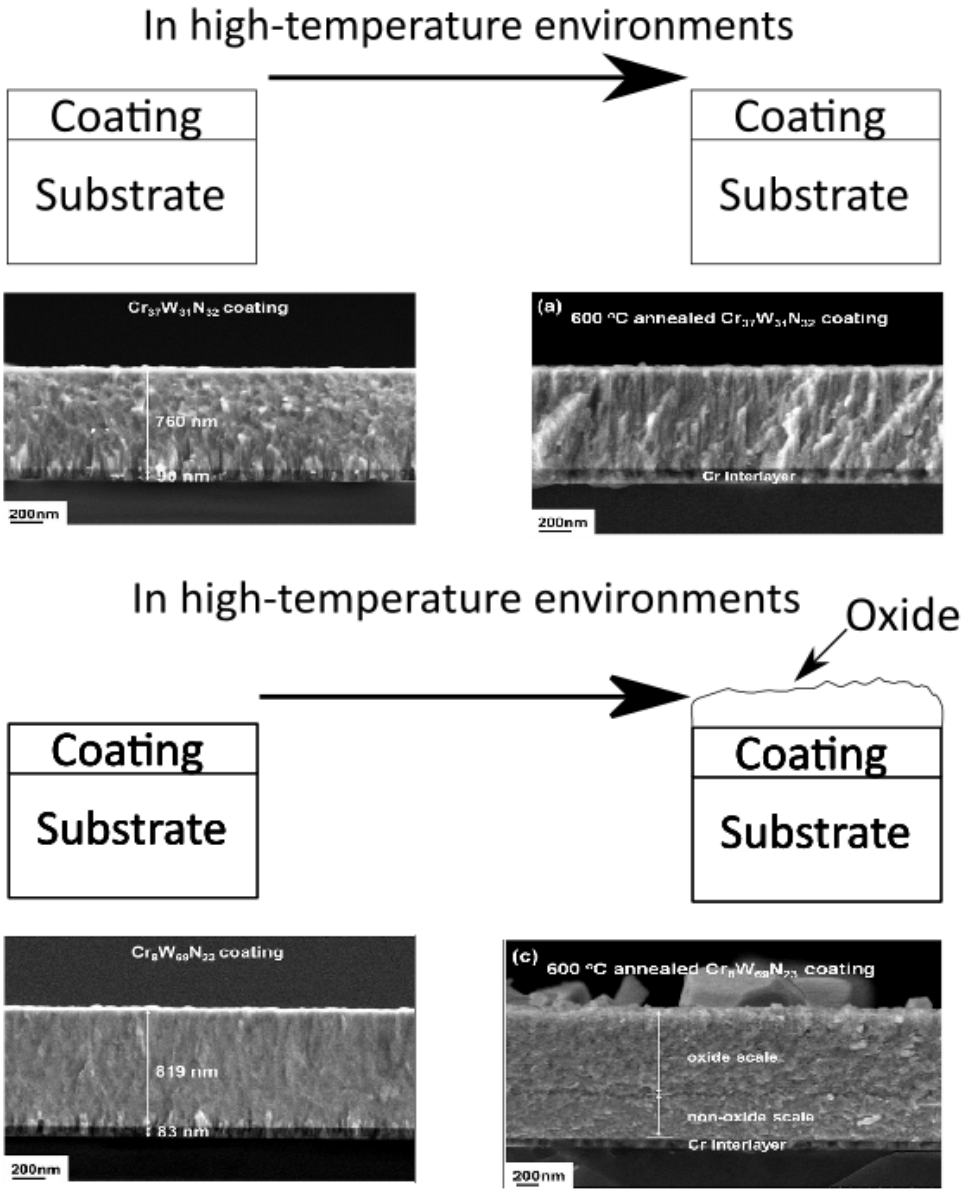

Figure 2.3: Schematics of oxide scale formation. SEM images are from [Chen et al., 2015a].

However, ceramic coatings could perhaps be a more affordable alternative for other consumer

products such as phone screen protectors that do not require as high form accuracy [Lee et al., 2018; Chang et al., 2017; Chen et al., 2015b].

2.3 Titanium-based coatings for glass molds

Titanium is a common base for ceramic coatings used in machining tools, examples include TiALN, TiBCN, TiBC, and TiB2 [Nunes et al., 2017]. Here TiALN is the most widely seen coating for the application in glass molding, its disadvantages are the aforementioned problems with reaction with the glass and increase in surface roughness [Klocke et al., 2010; Wang et al., 2019; Dukwen et al.].

2.3.1 Titanium-based coating patent

While titanium-based coating might not seem usable for higher Tg glass molding, a recent patent (march 2019) describes a well-performing coating consist of a layer of titanium, that forms TiC as the bottom layer and TiO2 at the top layer, which would be expected to form simply by annealing the sample.

The major difference from the norm is the choice of substrate, in this case being graphite rather than the usual tungsten carbide used in most other studies.

The patent further specifies to use a fine grain graphite to ensure proper mechanical and machinability properties. The graphite should have a similar coefficient of thermal expansion (CTE) to titanium to ensure the stability of the material system.

The demand for surface roughness is in the order of microns. Thus, combined with the fact that the testing glass of choice is that of Gorilla Glass ® it indicates a usage more target towards phone screens then optical components like lenses [Scoggins and Sheppard, 2019].

2.3.2 Formation of titanium-based coatings

PVD has become the most well-known and used method for applying titanium-based coatings. Within industry, PVD coating has been the primary technology for coating tools with titanium-based coating, such as TiAlN, since the 1980s. Chemical-based coating methods such as chemical vapor deposition and powder immersion reaction assisted coating has also been used as a method of applying the coating, but to a lesser degree [Erck and Maiya, 1998; Yin et al., 2005].

2.3.3 Observations regarding titanium-based coatings

In general, TiAlN is the most studied type of titanium-based coating but, there is a variety of other coatings that are also utilized.

The majority of studies focused on the wear and mechanical properties of the coatings [Nunes et al., 2017].

In general, the substrate used for this type of coating is either steel or similar alloys, or in the case of drilling tools carbides such as tungsten carbide. Therefore, a source of improvement of coating properties has been pre-treatment of the substrate such as nitriding and carburizing. The pre-treatment can be improved by applying a thin coating layer before to ensure, that the process does not cause degradation of the substrate. [Sharif and Rahim, 2007][Dobrzanski et al., 2010] [Marin et al., 2016] [Nunes et al., 2017] [Yumusak, 2019].

Titanium is known for its corrosion resistance, and titanium-based coatings are often used for corrosion protection. However, for optimum corrosion resistance, several parameters are needed to ensure good protection. Mainly, the integrity and structure of the coating can be weak points. As defects and pinholes in the coating can lead to diffusion of ions into the substrate which leads to damage. Due to imperfect coating deposition, thicker coatings can be needed to minimize the effect caused by defects in the coating [Liu et al., 2007; Yildiz et al., 2009; Matthes et al., 1991; Chaudhry et al., 2018].

To overcome this issue, post-treatment such as annealing can be used which can alter the structure to be denser, thus improving barrier properties by stopping either incoming or in the case of medical implants outwards diffusion of ions [Poon et al., 2005].

Another method that was found successful is the use of interlayers within the coating system. Interlayers have several advantages such as improving adhesion to the substrate and helping to isolate the coating and the substrate [Huang et al., 2007; Liu et al., 2007; Chaudhry et al., 2018].

An example of this is found in [Chaudhry et al., 2018] where effective corrosion protection of a silicon surface is shown by the usage of a titanium interlayer and a TiN top coating.

PVD applied TiN has a columnar structure that also can contain nanopores which can lead to pathways for reactive ions. The introduction of a titanium interlayer can act as a barrier and stop the deterioration of the substrate.

The concept is illustrated in Figure 2.4.

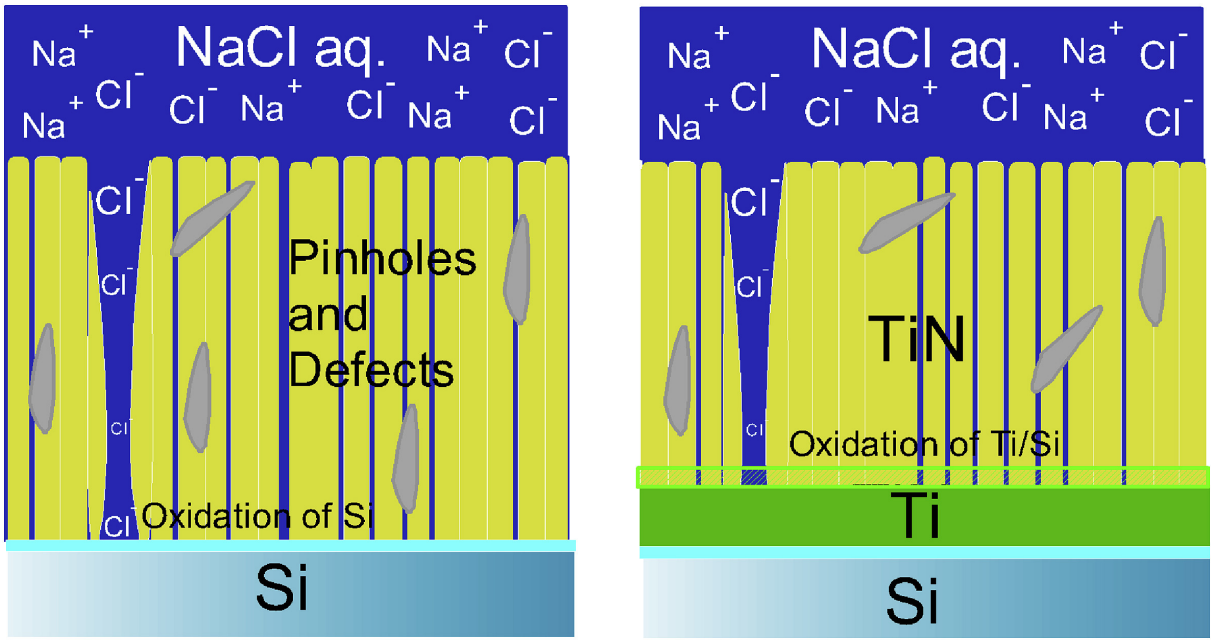

Figure 2.4: Illustration of corrosive action of silicon with TiN coating with and without Ti interlayer in 1 wt% NaCl solution. [Chaudhry et al., 2018]

Other industrial uses such as nuclear fuel cladding and high-pressure die-cast molds for aluminum components require good thermal properties [Nunes et al., 2017].

When looking into titanium-based coatings usage in high-temperature environments, studies have shown that TiALN has proven the best candidate with an oxidation resistance of up to 700°C [Park and Kim, 2002].

Further improvements of oxidation resistance has been found using multilayer structures, even the addition of thin nanolayers show improvements towards the thermal resistance [Zhang et al., 2020; Yan et al., 2019].

In [Yan et al., 2019] a multilayer structure consisting of TiAlN with interlayers of AlN is investigated. The interlayer thickness is varied from 1-5 nm. An optimum in surface roughness, hardness, and coefficient of friction is found when the interlayer of AlN is 3nm thick. Thus, while multilayer structures provides an improvement in thermal properties, it also requires high precision control of the composition.

Titanium-based films can have great variance in structure depending on deposition conditions. Thus, sputtering power, substrate temperature and sputtering pressure (pressure of inert gas during sputtering in the vacuum chamber) can affect the final film properties. The roughness of the structure is seen to increase with sputtering power. Grain size can also be observed to increase with an increase in sputtering power [Jin et al., 2009; Chawla et al., 2009; Einollahzadeh-Samadi and Dariani, 2013].

In a similar manner to sputtering power, substrate temperature, and sputtering pressure both also show an increasing trend towards grain size and surface roughness.

Yet, while the same tendencies can be seen across similar studies, DC magnetron sputtering on titanium of glass substrates, some differences are noteworthy. In [Jin et al., 2009] film thickness is the range of approx. 100 to 250 nm whereas in [Chawla et al., 2009] and [Einollahzadeh-Samadi and Dariani, 2013] the film thickness is the range of approx. 2-6 µm. This thickness difference significantly affects the roughness, in the former, it is only about 5 nm, while the latter is about 10-100 nm.

In [Jin et al., 2009] the structure obtained at low sputtering power (sub 200W) is described as amorphous-like due to the lack of obvious crystalline features, however in [Chawla et al., 2009] titanium film deposited using the same power can be observed to give a clear XRD signal, indicating crystallinity. It should be noted that in [Chawla et al., 2009] while the pressure is close to the same (12 mTorr vs 10 mTorr), the substrate is kept at 100 °C, compared to room temperature in [Jin et al., 2009]. Figure 2.5 and 2.6 show the comparison between the Atomic Force Microscopy (AFM) image of the film deposited at 100W and 150W from [Jin et al., 2009] and the SEM images from Chawla et al. [2009]. SEM image is used from [Chawla et al., 2009], as only the 3D AFM image is present in this paper, and it is easier to compare 2D images.

In [Jin et al., 2009] the sputtering power is increased up to 300W, and a crystalline structure is observed. The same type of crystallinity can be observed in [Chawla et al., 2009] also at 100W sputtering power, 100°C substrate temperature and 20mTorr sputtering pressure. AFM and SEM image comparision can be seen in Figure 2.7.

Thus, it can be seen that while general trends can be observed e.g increasing trend in surface roughness with increased sputtering power, individual parameters can not be decoupled.

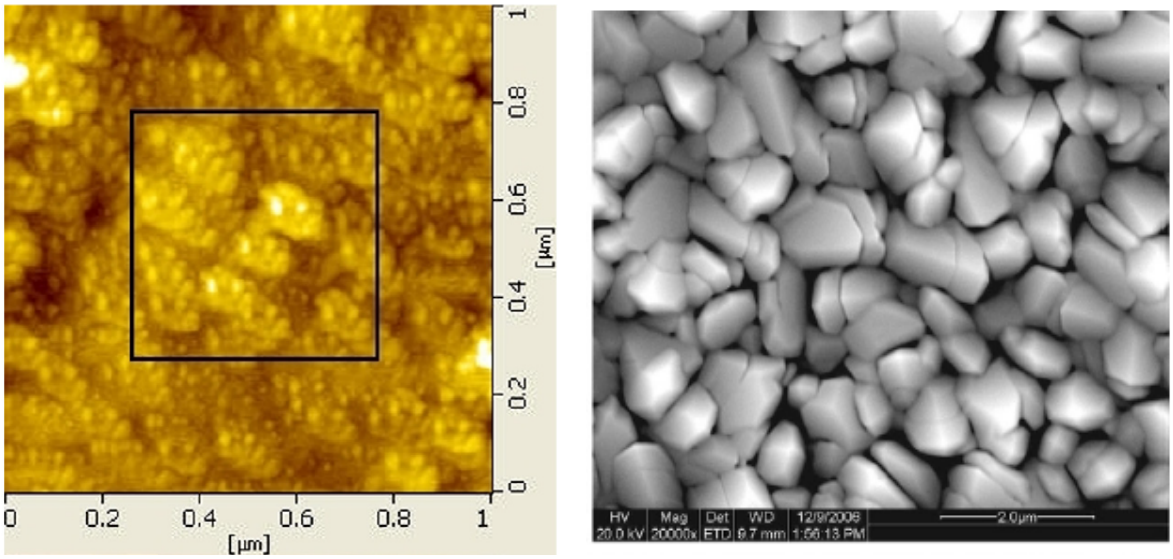

(a) (b)

Figure 2.5: a) AFM image of titanium film deposited on glass substrate at 100W, the black outline shows the zoomed area, presented in the original paper but skipped here [Jin et al., 2009] b) SEM image of titanium film deposited on glass substrate at 100W with a granular microcrystalline structure [Chawla et al., 2009]

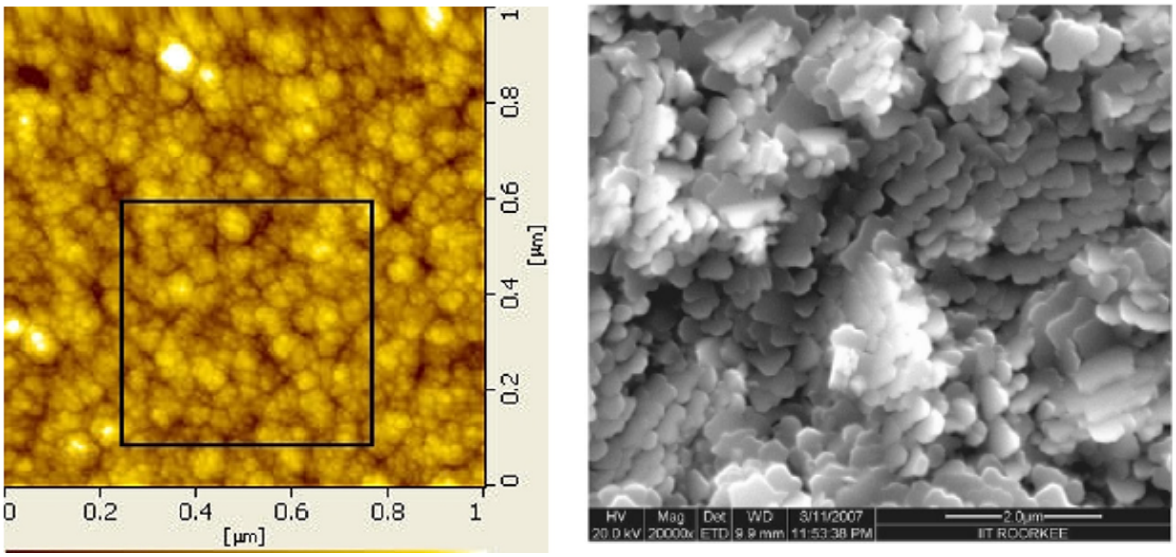

(a) (b)

Figure 2.6: AFM image of titanium film deposited on glass substrate at 150W, the black outline shows the zoomed area, presented in the original paper but skipped here [Jin et al., 2009] b) SEM image of titanium film deposited on glass substrate at 150W [Chawla et al., 2009]

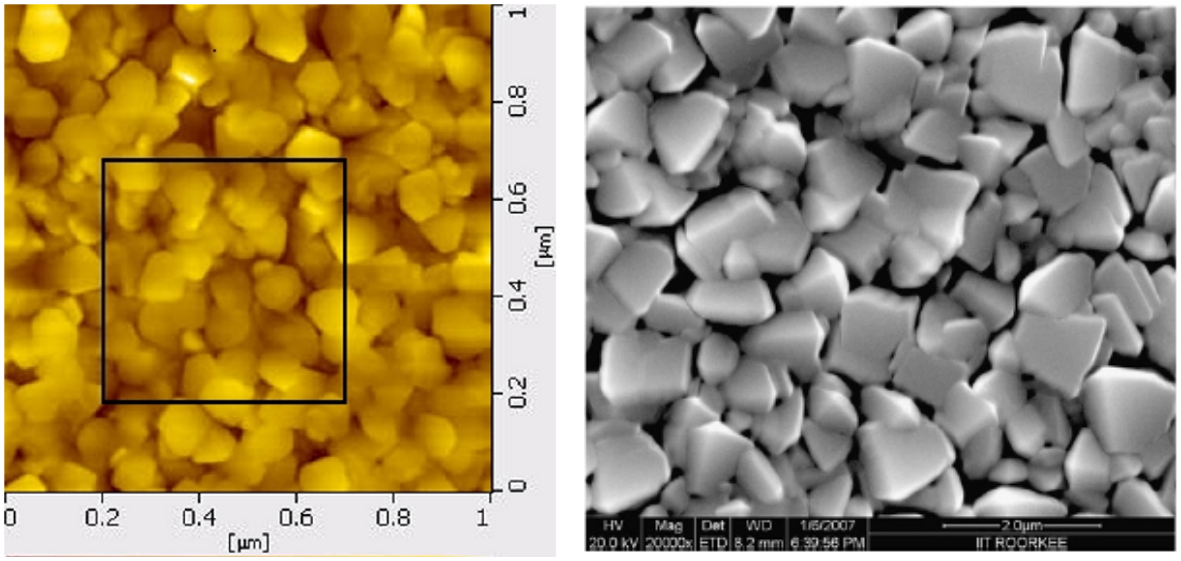

(a) (b)

Figure 2.7: AFM image of titanium film deposited on glass substrate at 300W, the black outline hows the zoom area, presented in the original paper but skipped here [Jin et al., 2009] b) SEM image of titanium film deposited on glass substrate at 20mTorr [Chawla et al., 2009] both exhibit crystal-like structures

2.3.4 Titanium-based coatings on graphite substrates

Graphite is widely used in industry due to its ability to withstand harsh high-temperature environments. However, its disadvantages are its susceptibility for oxidation at elevated

temperatures and its low wear resistance which severely limits its use as a structural material. To overcome this problem refractory metal such as titanium is used to increase oxidation resistance [Ameen and Wilayat, 2019; Mahmood et al., 2019; Rajput et al., 2018].

TiC and TiB_2 are examples of refractory metal coatings used on graphite. These coatings have been deposited by a large variety of methods.

Using high heat and powder either directly or in a cementation process with added elements has proven to be able to create coatings with good adhesion to the surface [Ameen and Wilayat, 2019; Yin et al., 2005; Yang et al., 2017] .

While cementation processes are more suited for large scale production due to economic concerns, good results have also been obtained by techniques more suitable for thinner coatings such as CVD and PVD.

In [Erck and Maiya, 1998] TiN, TiCN,TiC and TiB_2 coating were deposited unto graphite substrate using CVD. During pull testing, the coating/substrate interface never failed. The fracture always occurred in the graphite itself. Similar behavior was observed when deposited onto glass substrates. Thus, it could be seen that interfacial adhesion was excellent using CVD.

TiC coatings prepared by PVD deposition are well-studied [Fogarassy et al., 2018; Devia et al., 2011; Kumar et al., 2017]. In [Kaipoldayev et al., 2017] a TiC coating is formed by sputtering a graphite target unto a heated titanium substrate. The substrate temperature is varied from 700 to 1000 °C. In Figure 2.8 the Raman spectrum and XRD patterns for the different samples can be seen. It is observed that in the samples where deposition occured at substrate temperature of 1000 °C stable TiC, Ti_3C_2 and $Ti_3C_2O_2$ phases were formed. No amoruphous carbon and TiO_2 was observed. Thus, indicating Ti-C bondings between all the carbon atoms and titanium. Furthermore, in Figure 2.9 the SEM images of the samples where deposition occurred at substrate temperatures of 700 and 1000 °C, along with the EDX histogram of the samples are presented. This further indicates the full reaction of all the available carbon as it can be seen that the C content is increased. Comparing this with the phase diagram it can be seen that within a certain range of C/Ti atomic ratio only TiC is formed and no extra phase of Ti or C in the case of high C/Ti ratio is observed.

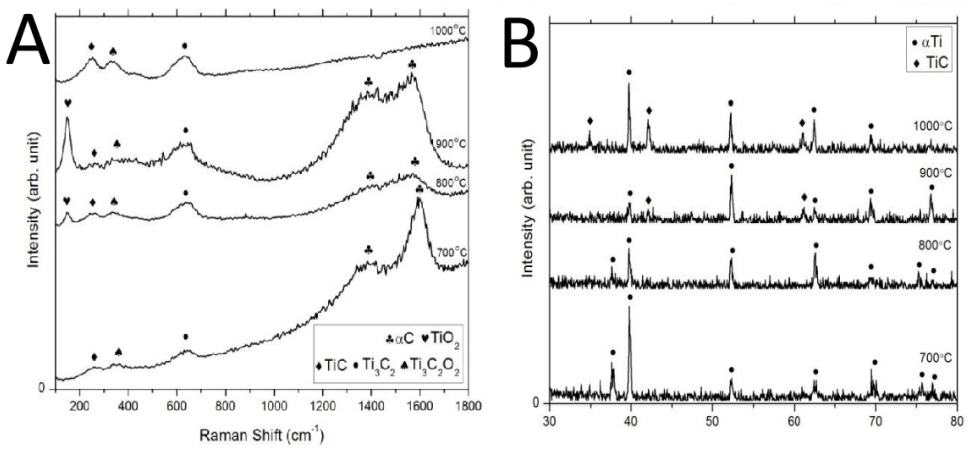

Figure 2.8: A) Raman spectrum of titanium samples coated with graphite at different substrate temperatures B) XRD pattern signal of titanium samples coated with graphite at different substrate temperatures [Kaipoldayev et al., 2017].

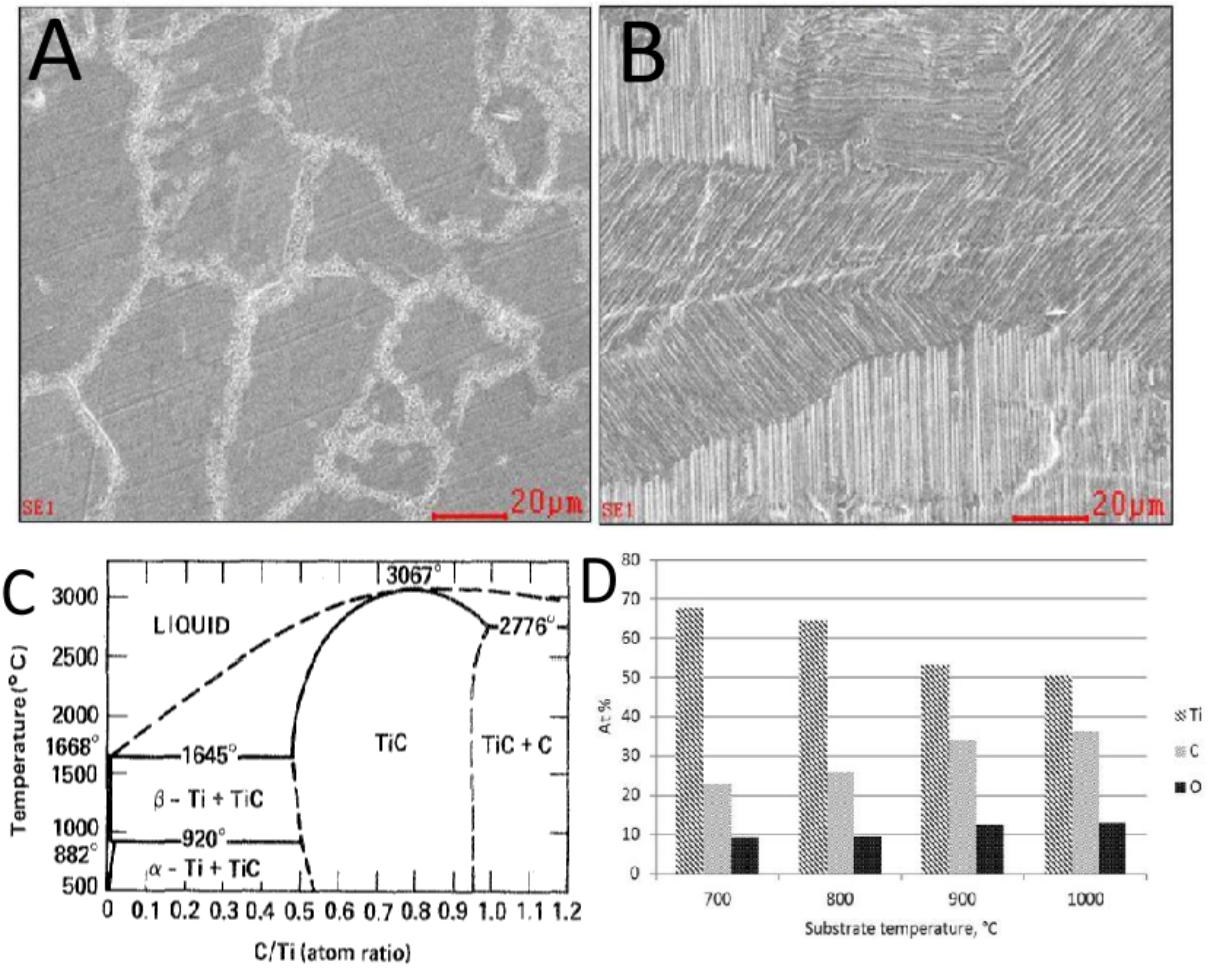

Figure 2.9: A) SEM image of titanium substrates coated with graphite at substrate temperature of 700 °C. B) SEM image of titanium substrates coated with graphite at substrate temperature of 1000 °C. C) binary phase diagram for Ti-C [Holt and Munir, 1986] D) Histrogram of EDX analysis of titanium substrates coated with graphite at varying substrate temperature [Kaipoldayev et al., 2017].

Thus, it should be possible to use PVD as a deposition method to apply a thin titanium coating, which then by annealing can be utilized to create a protective coating with good adhesion, while maintaining low thickness to ensure good form accuracy.

To summarize: While graphite and titanium-based coatings are not commonly used as a basis for high Tg glass molding, the literature supports the idea that they can be good candidates for the glass molding process at elevated temperatures. Major concerns are the lack of details regarding the film formation during deposition and subsequent annealing, and the breakdown of the film during thermal cycles.

3 Production and characterization methods

This chapter covers the production of samples and the methods used to characterize them.

3.1 Sample production

The material used in this work is a G077 type artificial graphite provided by NGS Trading and Consulting GmbH. It has an average grain size of 3 µm and it has a CTE of approximately $7.10 * 10^{-}6°C$. Furthermore, it is a hard graphite and therefore suitable to be used as a molding material as per Scoggins and Sheppard [2019].

The graphite was received as a small block, which then is cut into thin plates with dimension 10x10x1 mm to fit into the sample holder for PVD. The cutting is done by a Accutom 50 saw (Struers). An aluminum-Oxide cut-off wheel was used as well as a diamond saw. The cutting was done with water lubrication.

3.2 Physical Vapor Deposition

PVD refers to a variety of different thin film deposition techniques. Common for all of them is that the process occurs in a high vacuum environment, where a solid material (target) is vaporized, and the atoms/molecules are transported towards a substrate where the vaporized material condenses to form a film.

Several advantages are found with the technique including but not limited to: A large array of materials can be used for coatings, eco-friendly compared to chemical coatings, high purity of coatings, good adhesion and ability to design detailed structures.

A large variety of processes exist that all can be classified as PVD processes. Two common processes are magnetron sputtering and E-beam evaporation.

Magnetron sputtering is illustrated in Figure 3.1 and E-beam evaporation is illustrated in Figure 3.2.

Magnetron sputtering utilizes inert gas ions, typically argon, to bombard the target and thus vaporizing the material on the surface causing it to be released.

The process starts by forming an arc between two electrodes, one of the electrodes is the target.

As a plasma is formed by the ionization of the argon, electrons released from this event causes more ionization to occur. Thereby creating a self-sufficient plasma generation.

A magnet is placed behind the target and the magnetic field keeps the electrons entrapped which helps stabilize the plasma. This allows for lower operating pressure during the sputtering.

As the argon ions hit the target (cathode) atomic size particles are released. Thus, as the sputtered particles collide with the substrate surface they condense into a solid film.

In the case of E-beam evaporation, the target is heated by bombardment of electrons in a high vacuum. Once the evaporated material, in the form of atomic size particle, is released they clash with the gas molecules with the aim of increasing acceleration by creating a plasma. When they reached the substrate, a film is formed.

Evaporation has the advantage of high deposition rate, however, due to higher vacuum the deposited species energy is low which leads to less homogeneous film with lower adhesion. Thus, for thicker films evaporation is preferred.

While sputtering has a lower deposition rate, it does allow for far better control and film that have better adhesion and are more homogeneous.

Therefore, in this work sputtering is utilized as the method of film deposition as thin but highly controlled films are sought after [Shi, 2018; Baptista et al., 2018; Fuentes et al., 2019; Mitterer, 2014].

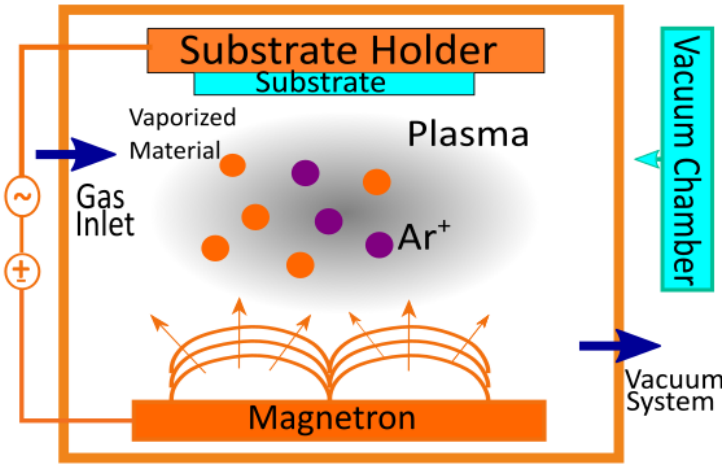

Figure 3.1: Schematic of Magnetron sputtering process

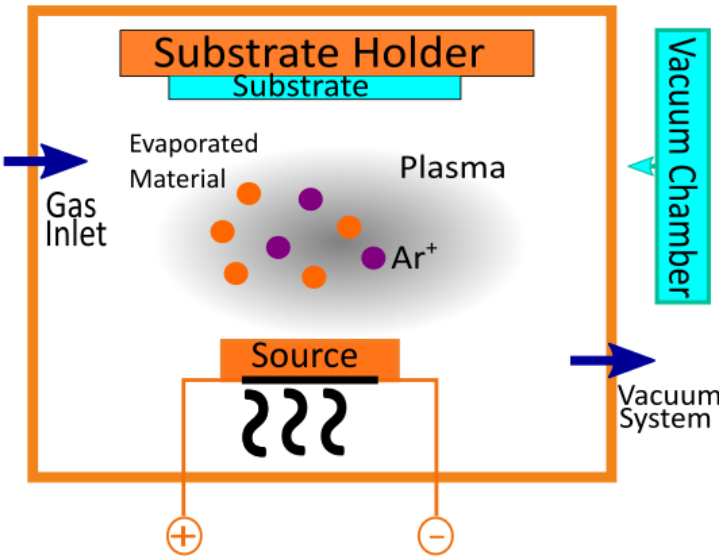

Figure 3.2: Schematic of E-beam evaporation process

3.2.1 Cryofox - thin film deposition system

The "Polyteknik Cryofox Explorer 600" PVD system can be seen in Figure 3.3.

Figure 3.3: Picture of Cryofox explorer 600

The cryofox is used to make thin films by DC magnetron sputtering in this project. The thin film

is produced at different thicknesses by increasing deposition time. For all depositions a reference piece of silicon is also coated, see Figure 3.4 for a picture of the sample holder.

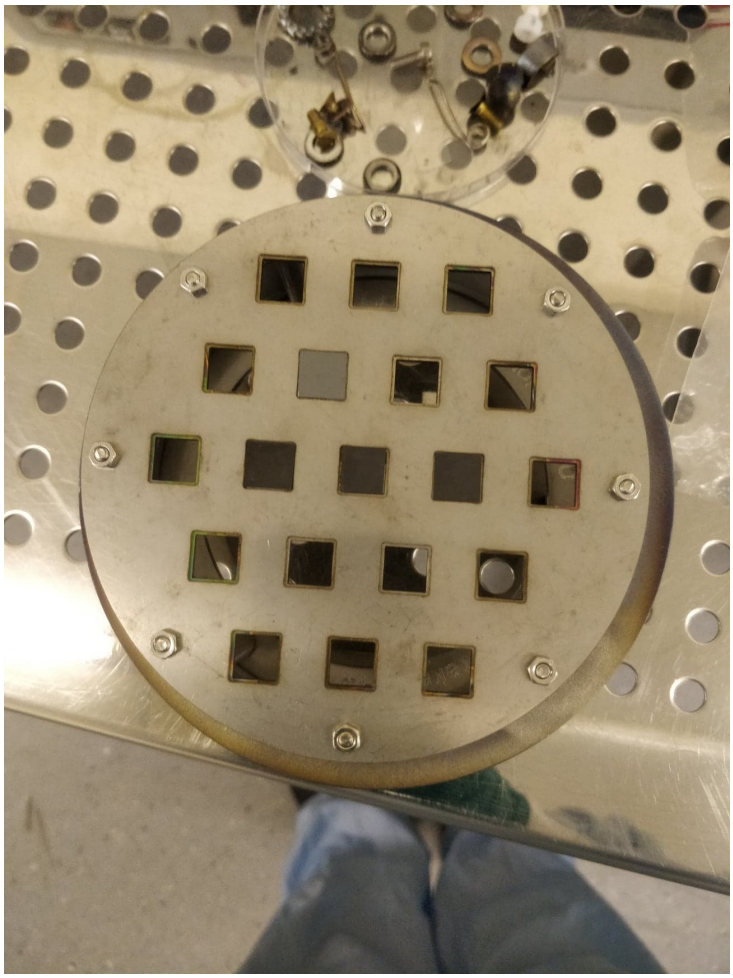

Figure 3.4: Sample holder with substrates for deposition

To check the thickness of the deposited films, a scratch is made down to the silicon substrate. It is then measured by a XP 2 stylus profiler (AMBIOS technology). This is done as there can be a discrepancy between the estimates provides by the microbalance crystal in the cryofox system and the actual thickness of the deposited coating.

Four types of samples were produced with different thicknesses. Samples with approx. thickness of 30 and 60 nm were made using the same sputtering parameters (power of 200W and 50sccm Ar), which corresponds roughly to a deposition rate of 0.7 Å/s. Samples with approx. thickness of 80 and 130 nm had issues during sputtering. For the case of 130 nm samples, it was found to be necessary to increase Ar flow up to 60 sccm Ar to counteract the loss of deposition. For the 80nm samples, Ar flow was further increased to 70 sccm. For 80nm and 130nm samples, a higher deposition rate of 0.8 Å/s was obtained.

3.3 Thermal annealing

A quartz tube furnace (Nabertherm) was used to anneal the samples. The coated samples were annealed for 1 hour in 1000°C under nitrogen flux. The quartz tube was first evacuated to a low vacuum (around 1 Pa), the tube was then filled with nitrogen gas. 1.5 hours were used to increase the temperature to the expected temperature. The samples were kept in a nitrogen atmosphere both during heating and cooling.

Since the films were developed for use in glass molding, it is of interest to study how the titanium coatings will behave in contact with glasses. For that small pieces of borosilicate glass were put on top of the samples and placed in the oven. The samples are then annealed for 20 minutes at 650 °C. Figure 3.5 shows the sample setup prepared for the annealing (contact test).

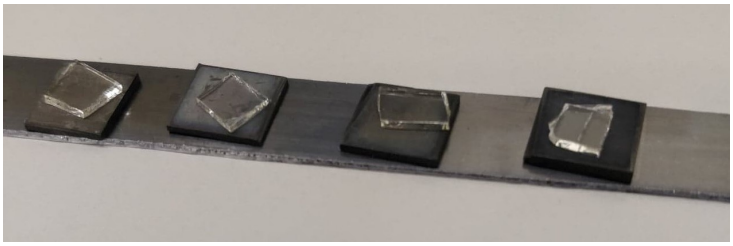

Figure 3.5: Picture of the setup used for contact test. Glass pieces on pure graphite (right) and graphite coated with titanium. A silicon bar is used a supporting stage.

The choice of temperature for the contact tests is based on common approach Tg + 120 °C [Wei et al., 2019; Zhu et al., 2015; Chao et al., 2013b]. Per [Chen et al., 2015a] 600°C is common during the production of most optical components. Thus, based on the aforementioned 650°C is chosen as the temperature for this experiment.

3.4 Atomic Force Microscopy

AFM is a widely used technique to measure topography and surface roughness.

There is a strong linkage between surface topography and the functionality of the coating. Here surface roughness is a significant parameter as it affects surface properties like adhesion, friction, and hydrophobicity. In general, the surface topography is a critical feature in various applications such as electrical, optical, mechanical, and thermal.

A typical AFM setup is illustrated in Figure 3.6.

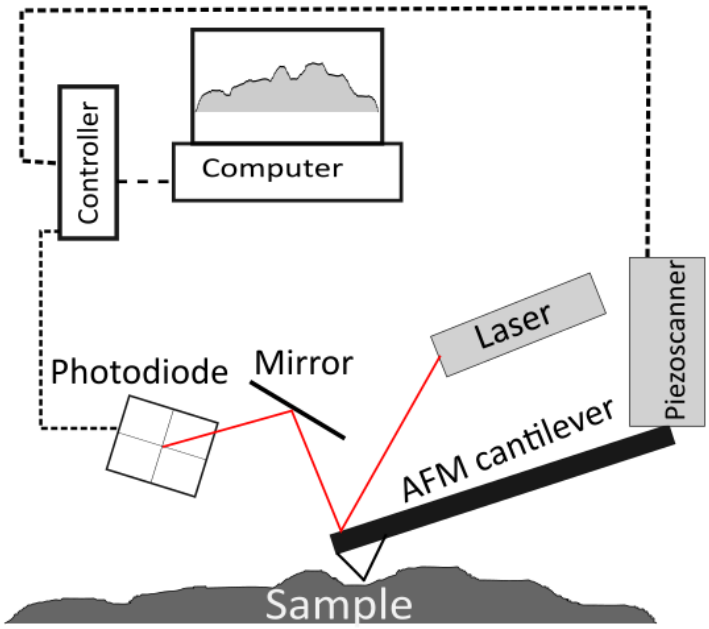

Figure 3.6: Schematic of a typical AFM setup

The basis of AFM is the use of a probe with a sharp tip, mounted on a piezoelectric scanner. Due to intermolecular force, the cantilever bends as it comes closer into contact with the sample. The deflection is monitored by a laser that is focused on the backside of the cantilever, and from there it is reflected onto a split photodiode. By tracking the deflection, an electric signal is generated that is converted by software into surface profiles.

The high precision of the method stems from the position control gained by the feedback loop. The cantilever scans over the sample line by line, whereby the topographic image is generated. Thus, by combining multiple line profiles a full 3D image can be generated.

3.4.1 Equipment

The AFM used in this project is a Solver Pro from ND-MDT. Tapping mode was used for the measurements and commercial silicon cantilever with tip curvature radius < 10 nm were utilized All data is processed using the Image Analysis 2.12 software (NT-MDT). Average roughness, Ra (ISO 4287/1) is obtained using the roughness analysis feature of this software.

3.5 Scanning Electron Microscopy

Another method to gain insight into the morphology of a sample is SEM.

A schematic of a typical SEM setup is seen in Figure 3.7.

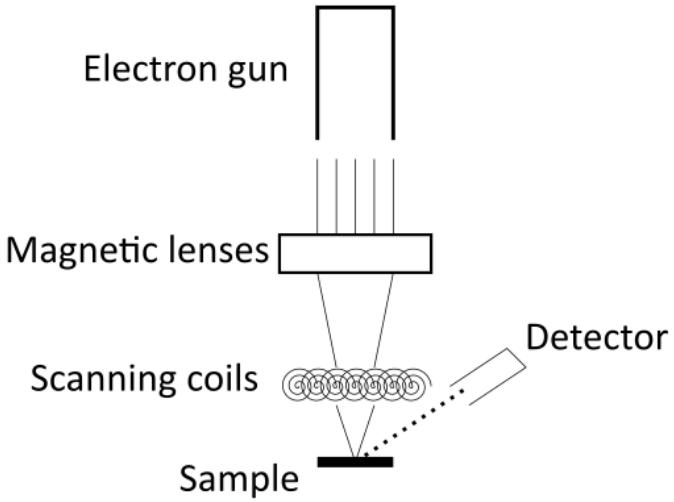

Figure 3.7: Schematic of a typical SEM setup

A electron gun fires out electrons that are accelerated, the electron beam is then focused by magnetic lenses into the scanning coils, which moves the beam in a rastering fashion thus allowing the user to scan a specific area of interest.

As the electrons are injected into the sample, the interaction causes a release of electrons and X-rays from the sample which are picked up by the detector.

The electrons are used to gain insight into the topography and different phases in the material.

A technique often combined with SEM is Energy-dispersive X-ray spectroscopy (EDX) which is a method used to gain insight into the chemical composition of the scanned material. This is done by analyzing the X-rays released by the injected electrons in the sample.

A tool often used together with SEM is Focused Ion Beam (FIB). The ion beam removes material in a controlled manner (milling), allowing for site-specific analysis. It can also be used in combination with a gas deposition, allowing for site-specific material deposition [Giannuzzi et al., 2004].

3.5.1 Equipment

A Zeiss XB1540 is used to take SEM images of the samples. It is also equipped with EDX and FIB which is used to gain insight into the composition of the samples and make a cross-section of samples. The FIB is also used for gas deposition of platinum for tracing purposes.

3.6 Optical spectroscopy

A LAMBDA 1050+ UV/Vis/NIR Spectrophotometer (Perkin Elmer) is used to analyze the glass samples after the contact test to see if there are changes in transmission due to possible sticking of the titanium films. The spectrophotometer was used in a standard double-beam configuration for transmission measurements in a wavelength interval between 320-850 nm. The spectra of the samples not subjected to the contact tests were used as a reference.

4 Results and Discussion

This chapter covers the results obtained from the characterization of the samples after the different processing steps.

4.1 Morphology and film structure

SEM and AFM were used to investigate the morphology and film structure of the samples. Figure 4.1 shows the SEM images of graphite samples under different magnifications.

It can be seen that the graphite has a "flaky" structure, which is especially well pronounced in Fig. 4.1b. It must be noted that such a surface morphology is an unexpected one, as it might create difficulties for homogeneous metal coatings.

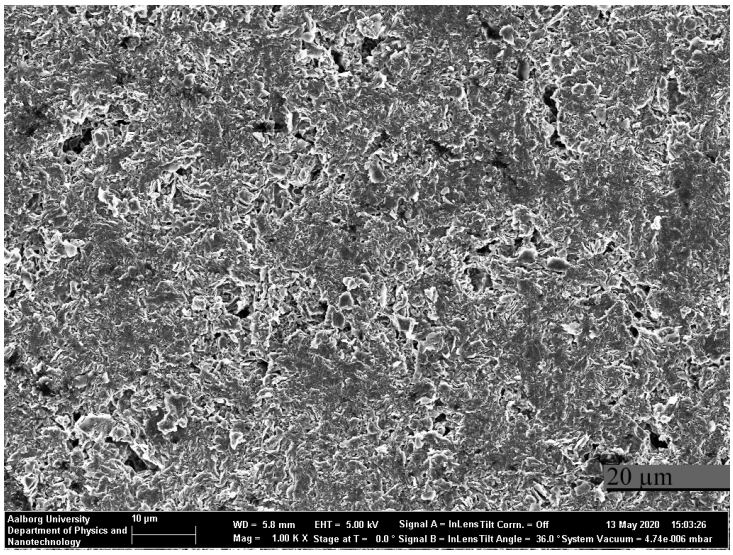

(a)

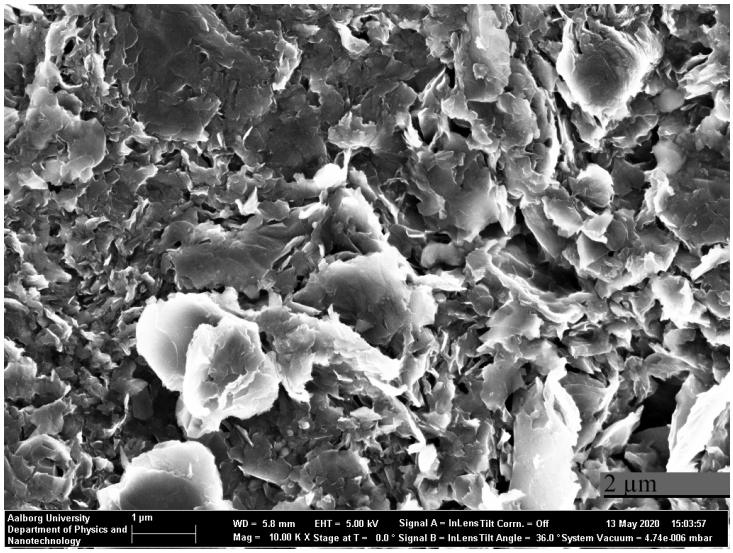

(b)

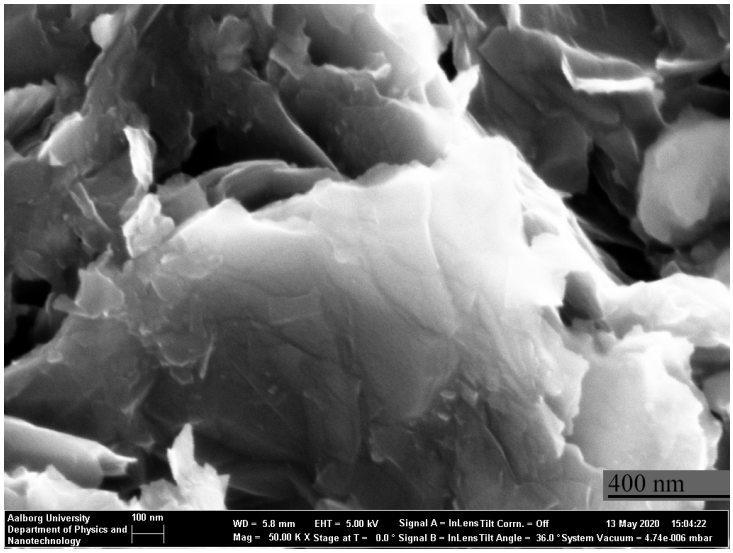

(c)

Figure 4.1: SEM images of graphite with different magnifications. See scalebar.

Figure 4.2 shows the AFM image of the graphite samples. The same texture is seen, however, the morphology looks a bit smoother, which is related to the scanning technique used in AFM. On the other hand, the advantage of AFM is in providing a precise topography profile with a clear indication of height difference as can be seen in Figure 4.2b. The image presented in Figure 4.3 shows a dark valley in the middle. The height difference across the scan area is over 3µm. Taking into account that the length of cantilever tip is about 4-5µm and it has a conical shape with sharp tip but relatively large diameter on the other side, it might be that the tip is not able to reach the bottom of a valley.

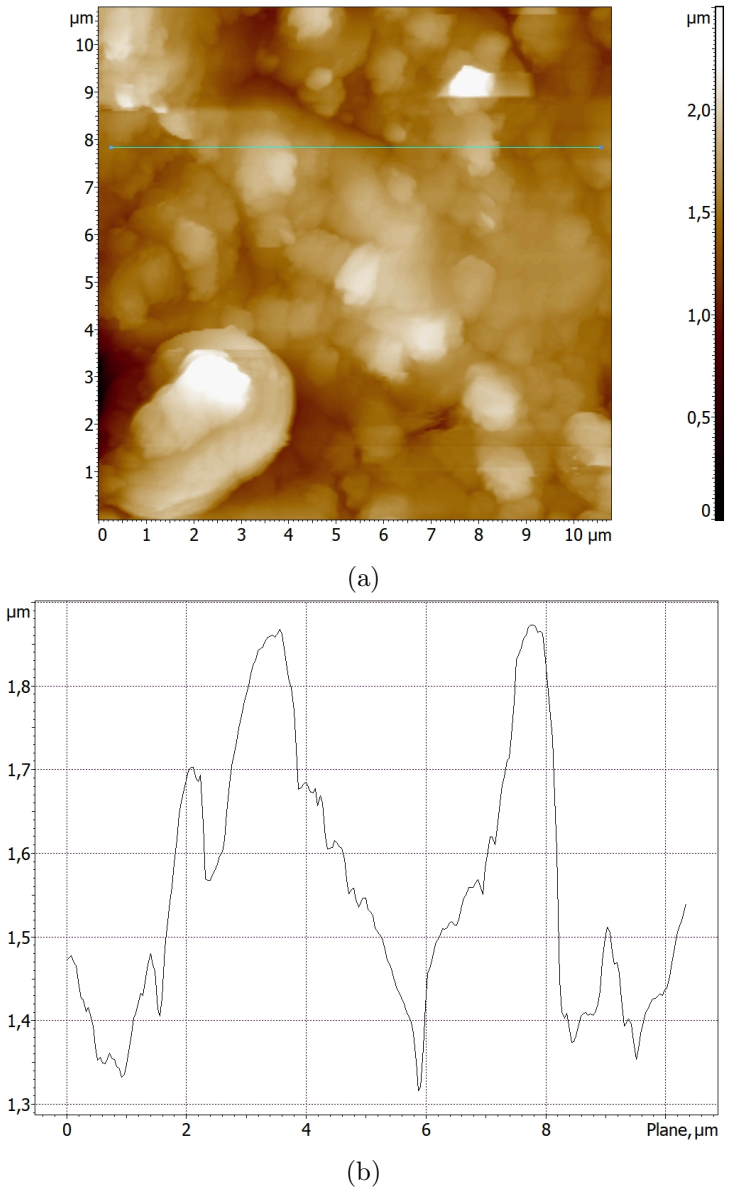

Figure 4.2: a) AFM image of graphite sample and b) topography profile along green line indicated in a)

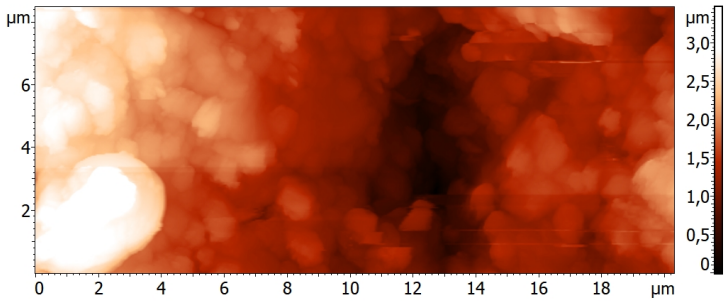

Figure 4.3: AFM image of graphite sample

Data on graphite roughness were obtained for the samples. However, there were few images and some of the images were of low quality, due to a large amount of "noise" in the image. Table 4.1 presents selected roughness data obtained for the images.

Table 4.1: Selected roughness data for AFM images of graphite

Parameter/AFM image	Image 1	image1*	Image 2	Image 3	Image 4
Max height	3284 nm	2811 nm	2500 nm	3908 nm	4772 nm
Average	1539 nm	1539 nm	1558 nm	1612 nm	2066 nm
Average Roughness, Ra	215 nm	217 nm	188 nm	330 nm	590 nm
image scan size	20x20µm	11x21µm	7x7µm	21x21µm	23x40µm

Image 1* corresponds to Figure 4.3 and image 1 corresponds to the non-cropped version which can be seen in Appendix A. Image 2 corresponds to Figure 4.2a. Image 3 and 4 corresponds to another graphite sample and a larger scan area of image 1. Both can be found in Appendix A.

Comparing image 1 and image 1* the average roughness remains the same while there is a decrease in the max height.

Image 1 and 3 have the same image scan size. However, it can be seen that overall there is an increase in the roughness data. This matches with the increase in noise in the image, as the "noisy" lines often corresponds to higher z-data points.

Similarly, image 4 has an increase in all roughness data. However, this can be expected based on the structure as seen in the SEM images. Since a larger contrast will naturally arise as the images spans over multiple "flakes".

Image 2 has a lower scan size, but also far less noise than the other images.

Comparing with literature, the commonly used tungsten carbide substrate is polished prior to

deposition and is expected to have a Ra value of less than 5nm [Klocke et al., 2016; Chen et al., 2006; Wei et al., 2019].

Thus, it is found that the graphite surface is far rougher than the standard set for optical components form accuracy. To get a numerical value that can be considered representative for the whole sample, more images are needed. Yet, considering the morphology of the sample is already known to be quite "rough" the actual numerical value does not matter much as the morphology that is identified.

4.1.1 As-deposited film

Figure 4.4 shows the SEM images of as-deposited 130 nm film. It can be seen that the as-deposited film has a nanogranular structure and covers the surface. Figure 4.5 shows the AFM image of the as-deposited film on graphite and silicon. It can be seen that in both cases the coating has the same nanogranular structure. The nanograins are very clearly seen on the silicon substrate because of the very smooth surface but a bit worse for the case of graphite substrate with very high roughness.

The nanogranular structure seen on silicon matches findings in literature [Brama et al., 2005]. A lack of epitaxial growth is expected based on the lattice mismatch between silicon (FCC) and titanium (HCP) [NIST; Barksdale, 1968]. As for film formation on graphite, while both titanium and graphite has a HCP strucutre, there are difference in the lattice. For graphite $a_0 = 2.45$ Å and $C_0 = 6.70$ Å [Nicklow et al., 1972] and for titanium $a_0 = 2.95$ Å and $C_0 = 4.68$ Å [Wood, 1962]. Also, the graphite used is "artificial" graphite, which is isotropic. Thus, it is likely that this leads to further stacking errors.

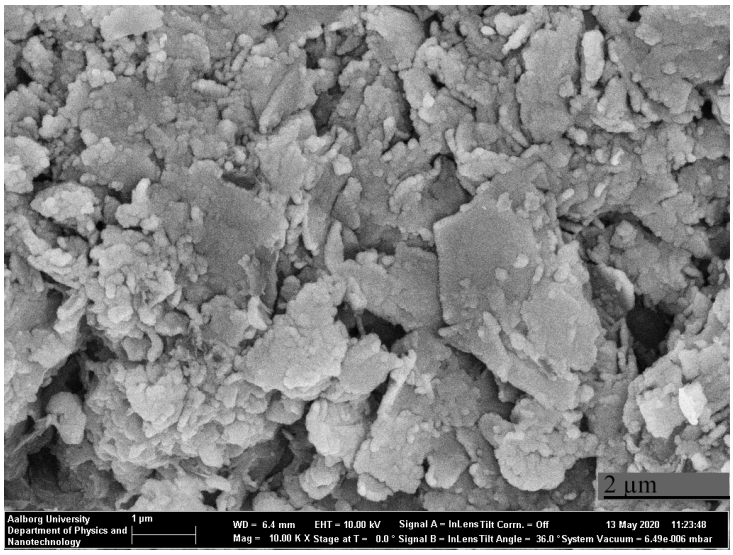

(a)

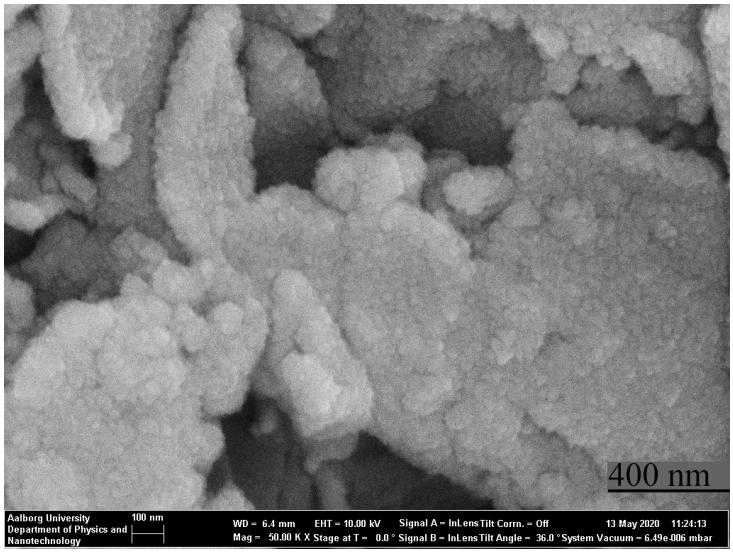

(b)

Figure 4.4: SEM images of 130nm film as deposited with different magnifications. See scalebar.

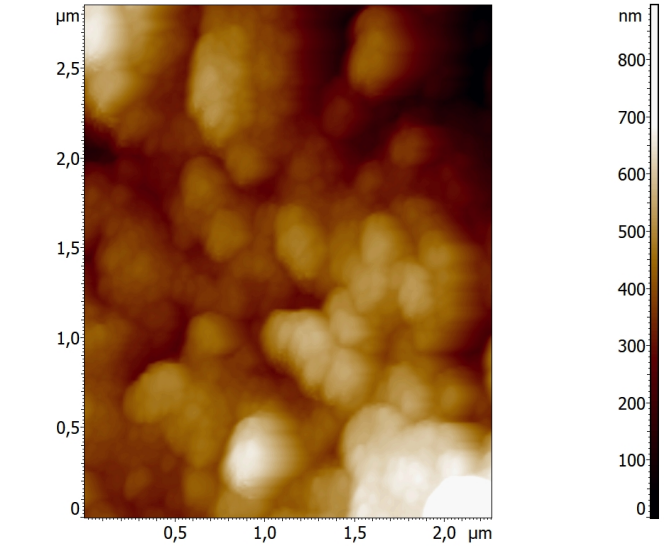

(a)

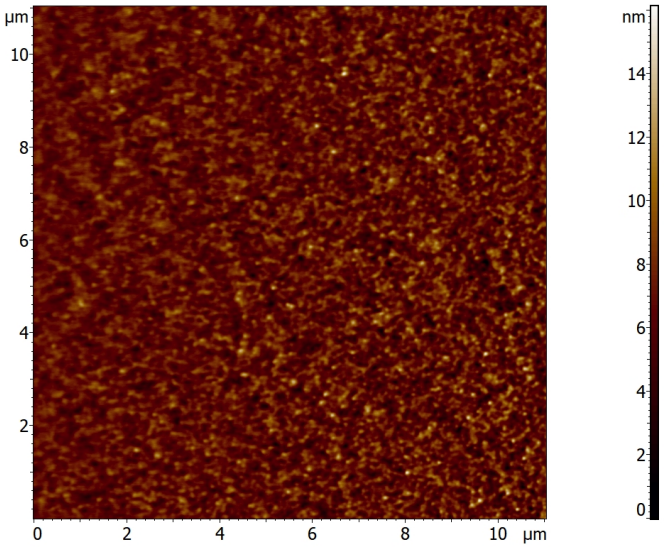

(b)

Figure 4.5: AFM images of 130nm film as-deposited on a) graphite substrate b) silicon substrate

4.1.2 Annealed samples

After annealing it can be seen in Figure 4.6 that the films have changed from a nanogranular structure to a nanocrystalline one. Comparing the 80 and 130nm films deposited on graphite substrates it can be seen that the 130nm film is denser and more coherent.

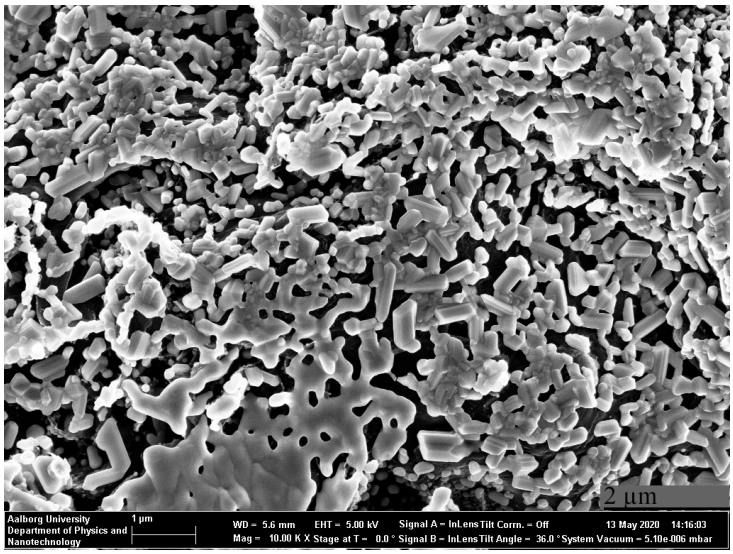

(a)

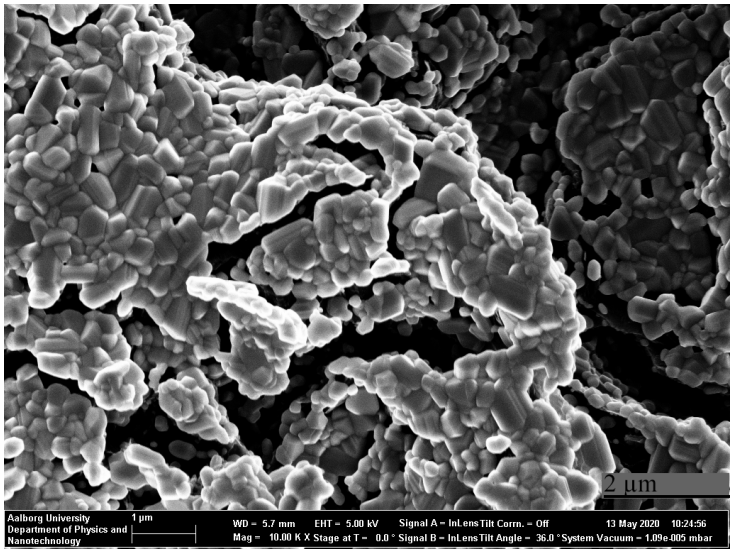

(b)

Figure 4.6: SEM images of a) 80nm and b) 130 nm samples after annealing at the same magnification. See scalebar.

It can be observed that the corresponding AFM images do not show this crystallinity, as seen in Figure 4.7. The reason for this is unclear.

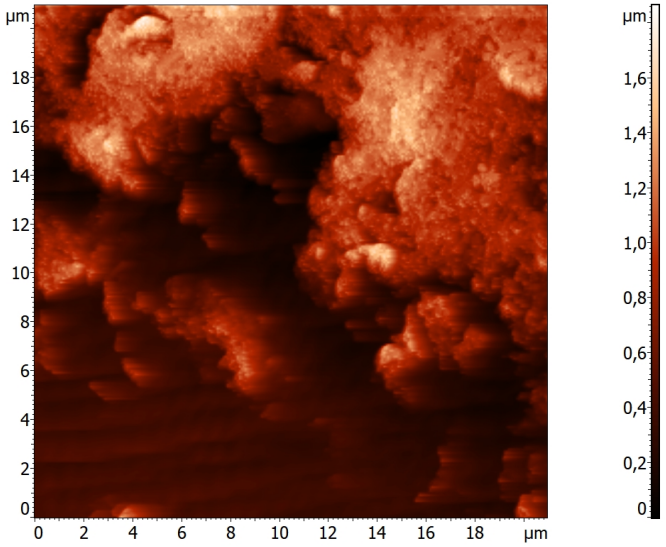

(a)

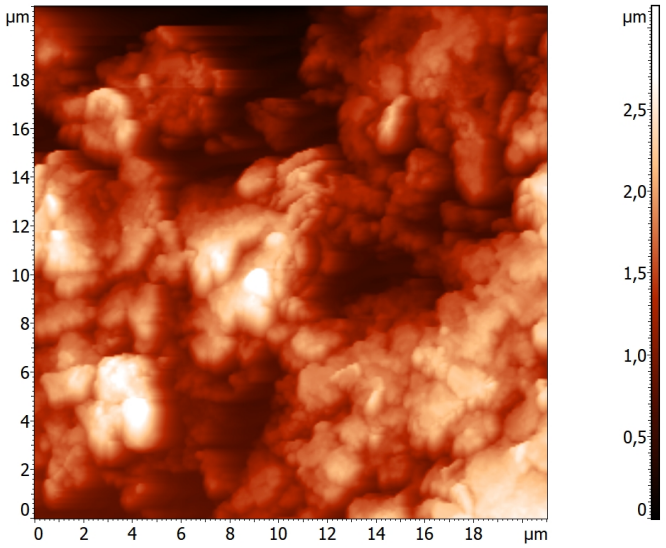

(b)

Figure 4.7: AFM images of a) 80nm and b) 130 nm samples after annealing

The film deposited on silicon substrates was also annealed and analyzed. It can be seen in Figure 4.8 that the film also changes into nanocrystallites.

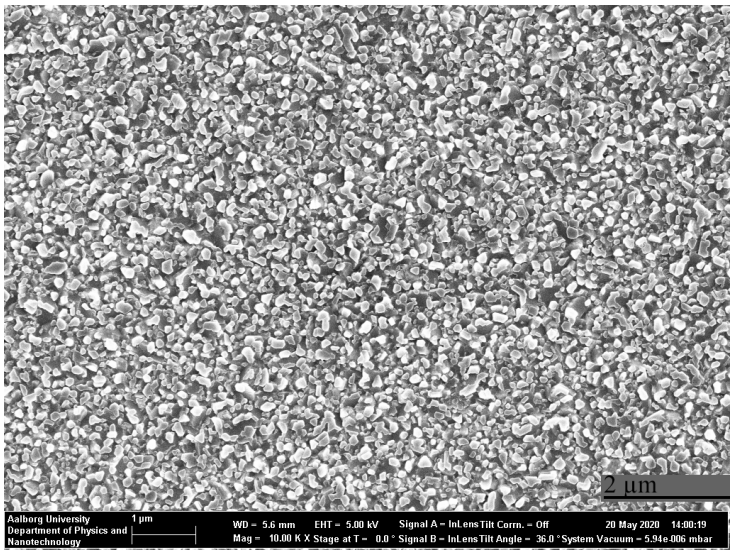

(a)

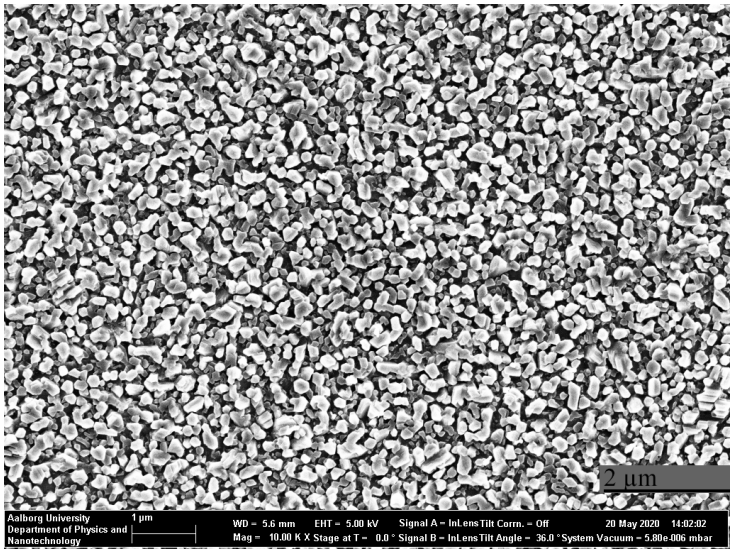

(b)

Figure 4.8: SEM images of a) 80nm and b) 130 nm film deposited on silicon substrate after annealing. See Scalebar

The annealed film on the silicon substrate can be seen to match the film seen in [Brama et al., 2005]. In [Brama et al., 2005] titanium film with thickness 450-1140 nm are deposited onto silicon substrates and subsequently annealed at temperatures from 600-900°C to make rutile films. The annealing time for 600°C was between 5-50 min. While it was kept constant at 20min for the other annealing temperatures. It was observed that the films had a granular structure as deposited. For shorter annealing time and temperature, a growth in granules size was observed. However, over a certain threshold of either time or temperature (depending on the film thickness) a change occurred in the film which then became denser and smoother with refined grain structure. This was attributed to the full transformation of titanium to rutile. Samples annealed at lower temperatures, contained Ti-Si intermetallic phases. This effect was decreased with lower thickness and higher temperatures. A film with a thickness of 450nm annealed at 900°C for 20 minutes

showed a complete transformation into rutile without any other phases present. In another study [Ting et al., 2002] a 170nm film is annealed 1h at 1000°C in which shows a complete transformation to rutile.

Thus, considering the film thickness, annealing time and temperature used in this project a change from titanium to rutile would very likely be the case if a similar atmosphere was used.

However, in this project nitrogen atmosphere is used, and thereby the amount of oxygen present is significantly reduced. Per [Chen et al., 2014] commonly in PGM process there is a small amount of oxygen present (15 ppm) during the nitrogen flushing Yet, oxygen diffusion can still occur in these conditions.

A study that could indicate the this technique would still cause oxidization is [Dai et al., 1999]. In this study, 100nm titanium film is shown to be annealed under argon flux at 500-700°C and show transformation into rutile as well. The procedure used is similar to the one used in this project, where first the quartz tube is evacuated to a low vacuum and then argon flux is used through the heating and cooling of the samples. It should be mentioned that similar studies all do annealing in air and not using argon flux or similar setups.

Thus, the change from nanogranular structure to crystalline can perhaps be attributed to the change from titanium to a rutile phase. However, it should be strongly empathize that this is based on circumstantial evidence only.

While a similar logic could be applied to the graphite samples, examples of titanium coating on graphite are more limited. Thus, it is not easy to compare with existing literature.

[Bakri et al., 2017] shows a TiO_2 film transformation after annealing, here it can be seen that the change from an even nanogranular structure to a more crystalline structure occurs by densification, in a very similar manner to the results obtained in this project. The same is seen in [Hou et al., 2003] where after annealing at over 900°C the film transforms into rutile with an increase in particle size to around 300-500nm. This change is expected as rutile is the most stable polymorph of TiO_2 and at elevated temperatures over 800°C other polymorphs of TiO_2 transforms irreversibly into rutile [Greenwood and Earnshaw, 2012; Diebold, 2003].

It should be noted that both papers start with a $Ti0_2$ film that transforms from anatase to rutile. This process is different than the one observed in [Brama et al., 2005] where it is a process straight from titanium to rutile. Although, at lower temperatures dissolution of oxygen in α-Ti lattice was observed by XRD. In [Ting et al., 2002] the reasoning for the lack of anatase phase is given as the oxidation time to reach a near-stoichiometric ratio is shorten under the experimental conditions. Interestingly in this study, a similar morphology i.e. more coherent is seen compared with [Brama et al., 2005]. The substrate used is quartz glass.

Thus, the difference in film morphology is likely to be attributed to some substrate effects. In [Dai et al., 1999] epitaxial growth of rutile on silicon is indicated by EDX data.

In accordance with [Dahotre et al., 2001] titanium has a high work of adhesion on graphite at

elevated temperatures due to chemical interactions and as such is expected to have good wetting on graphite. In [Brama et al., 2005] Ti-Si formation is observed during annealing under certain circumstances, perhaps an interaction between titanium and graphite could occur during the annealing and causing better coherence due to interaction between substrate and film.

However, this explanation appears unconvincing as an attempt was made at making a cross-section for the 130nm graphite sample using FIB (see appendix B for images), which gave no indications of the titanium carbide layer formation.

A large difference between the graphite and silicon substrates is their surface roughness. Ra is approx. 1 nm for the silicon substrate while it approx. 200nm for the graphite substrate. Considering samples of the same area, greater surface roughness leads to a larger real surface area. As a larger area is exposed to the air, it means that oxidation can take place faster [Wang et al., 2015]. Considering that the tendency seen for rutile formation is densification and larger crystallite size as temperatures increase, an explanation could be that the film on top of the graphite has been oxidized more and thus, has reacted further to create a denser film with larger crystallite size.

Using pixel measurements the approx. average size for the 130nm films crystal on graphite is 389nm and for the film annealed on the silicon substrate the approx. average is 235nm.

To restate per [Brama et al., 2005] at a certain threshold regardless of thickness, there is a change in the structure causing the film to become smoother and denser. Perhaps the film deposited on the silicon substrate is only in the process of densification, as compared to the counterpart deposited on the graphite substrate.

4.1.3 After contact test

After the contact test, it was not possible to see any residue of titanium or carbon on the glass. The SEM images show no noticeable difference except in the 130nm sample where at "high" magnification the presence of small sphere-like objects on the crystal can be observed as seen in Figure 4.9. Its origins are unclear. Interestingly using pixel measurements it can be seen that there is an increase for the approx. average of 389nm to 573nm for the 130nm film, which could indicate further oxidation and development of the rutile phase. Despite the lack of an apparent reaction between the samples and the glass, there is a possibility that some of the nanocrystals can stick to the glass. Thus, optical transmission measurements are needed to investigate if some interaction happened or not.

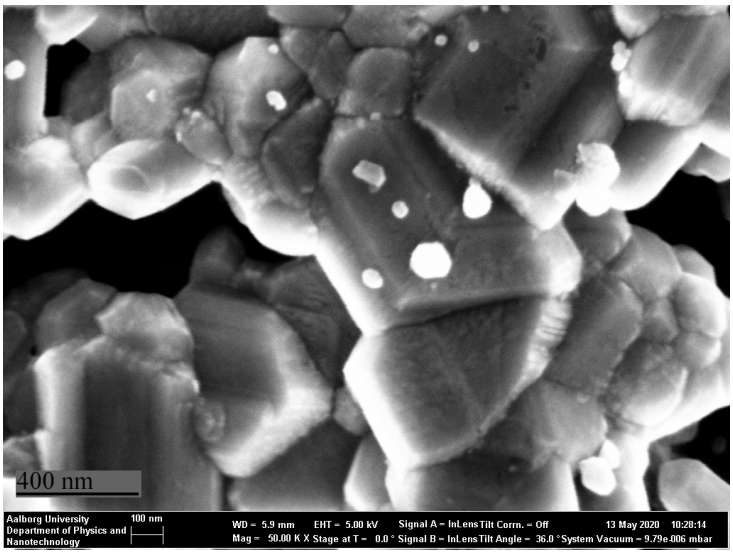

Figure 4.9: SEM image of 130nm film after contact test at "high" magnification. See scalebar

4.2 EDX analysis

EDX is used to identify changes in the chemical composition of the samples. Based on the used 10kV electrons, the X-ray signal would be expected from a depth of up to 1 micrometer.

For each analyzed sample, four areas were chosen to be analyzed to get an average of the sample, as there can be local variations in chemical composition.

Figure 4.10 shows the SEM image of the graphite sample with the four indicated areas. Each area corresponds to a EDX spectrum. Figure 4.11 is the EDX spectrum that corresponds to area 1 in Figure 4.10. Table 4.2 shows the atomic data for all four areas of graphite.

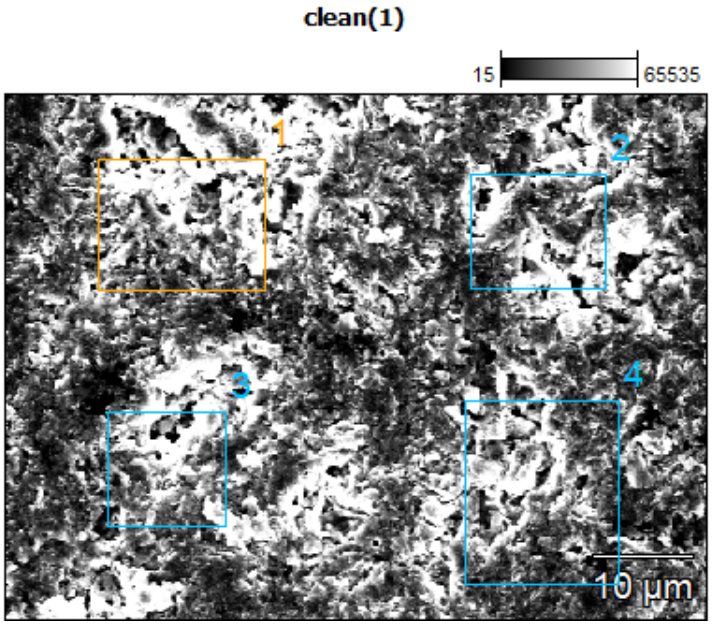

Figure 4.10: SEM image of graphite sample with four indicated areas used for EDX analysis

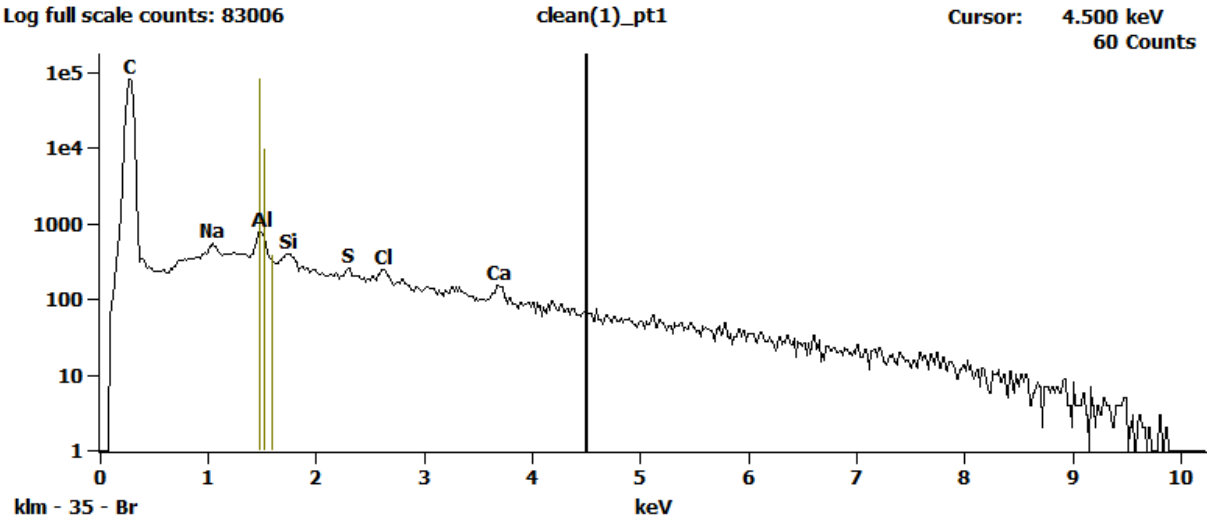

Figure 4.11: EDX spectrum corresponding to area 1 highlighted in figure 4.10

Looking at Figure 4.11 it can be seen that C is the dominant element in the composition (note the y-axis is logarithmic). Trace elements of Na, Al, Si, S, Cl, and Ca are seen in the spectrum.

Table 4.2: atomic % data for graphite substrates, average ± standard deviation is given for each of the 4 measured areas

Area/element	C-K	Na-K	Al-K	Si-K	S-K	Cl-K	K-K	Ca-K
clean pt1	99,31	0,13	0,22	0,08	0,05	0,08	0,00	0,12
clean pt2	99,52	0,09	0,13	0,06	0,00	0,08	0,00	0,12
clean pt3	99,42	0,12	0,15	0,06	0,00	0,09	0,03	0,13
clean pt4	99,56	0,09	0,19	0,00	0,00	0,07	0,00	0,09
Average ± SD	99,45±0,10	0,11±0,02	0,17±0,03	0,05±0,03	0,01±0,02	0,08±0,01	0,01±0,01	0,12±0,02

Looking into the atomic % data in Table 4.2 it can be seen that the trace elements are all under 0.5 % with the highest average element being Al. This can be contributed to the cutting process as an aluminum-oxide cut-off wheel is used for the initial cutting. A diamond saw with water lubrication is also used which can explain the presence of the other elements as salts and sulfates are commonly found as minerals in water. The local variation in composition can be seen for S and K as they each only appear in one of the scanned areas, note K is not present in the Figure 4.11.

Similar analyses were performed for the graphite after contact to see if there was a change in composition. The spectrum can be seen in Figure 4.12. Due to a software error, it was not possible to get any numerical values for oxygen presents observed (the values were set as zero). However, the atomic % registered for Na peak is 0.31 % so approx. the same amount of oxygen is probably present. The other spectrum for graphite in contact shows similar oxygen levels and trace elements, while trace elements are absent in two other measured spots (not shown). Thus, it indicates that some oxidation has occurred during the contact which would be expected, as graphite is known to easily oxidize at 400°C and above [Mahmood et al., 2019].

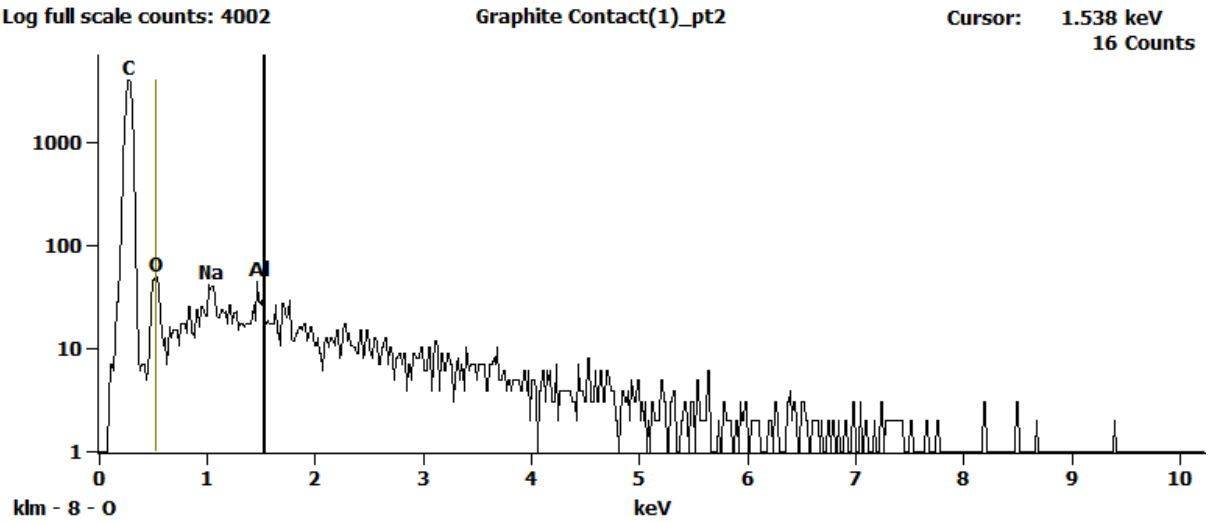

Figure 4.12: EDX spectrum for graphite after contact test

Table 4.3 shows the average data for oxygen and titanium atomic % for the 80nm and 130nm as-deposited, annealed and after contact test samples. The data is selected as it is the most interesting in terms of analysis. The full data-sheets can be seen in Appendix B. For all samples high carbon content and trace elements matching those found in the substrate are present.

Table 4.3: Selected average ± standard deviation atomic % data for 80nm and 130 samples as-deposited, annealed and after contact test, respectively

Sample/Element	Oxygen	Titanium
80nm	6,14±0,32	7,59±1,76
80nm annealed	12,51±1,68	5,45±0,73
80nm contact	16,12±2,14	6,75±0,66
130nm	8,57±0,68	13,40±0,51
130nm annealed	17,68±7,78	10,53±3,08
130nm contact	25,94±3,88	12,86±2,48

Considering the EDX signal is collected from a depth of up to 1 µm in the sample carbon is expected to be the main element observed and as thickness is increased the titanium content is expected to increase. However, it can be observed that after thermal treatment there is an increase in oxygen and a drop in titanium content. If oxygen was only present in the surface layer, the content should remain somewhat the same across the measurement. However, a significant increase in oxygen is observed after annealing in 130nm film compare to the 80nm film. This could be an indication that the titanium nanocrystals became totally oxidized.

Furthermore, the O/Ti ratio is roughly 2/1 for the measurements obtained which indicates the presence of TiO_2. Thus, the relative increase of oxygen and the relative decrease of titanium can be attributed to oxidation.

4.3 Optical spectroscopy measurements

Optical spectroscopy was done to gain insight into if there had been interaction between the coated samples and the glass during the contact test. Pure Graphite substrate was used as a control sample. The glass transmission was analyzed. Figure 4.13 shows a section (75-79 % Transmission) of the spectrum for the transmission measurement done. The full spectrum from 320 to 850nm can be seen in appendix D. All samples followed the same tendency with a drop in transmission as the wavelength decreases, which is a typical behavior for a glass.

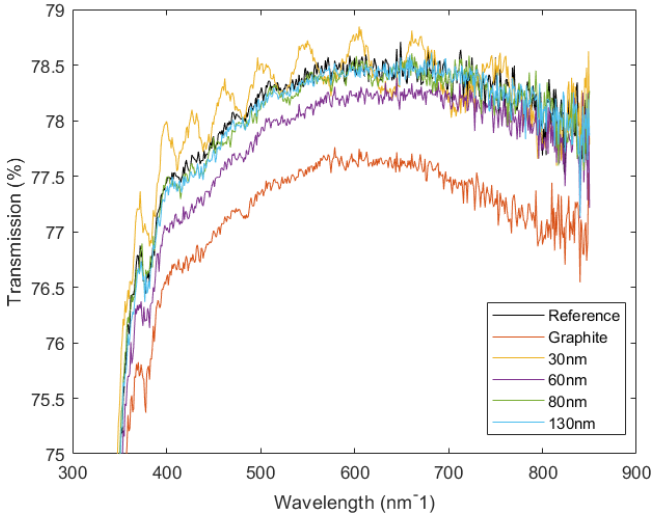

Figure 4.13: Section of the spectrum's done for samples after the contact test

The glass which was in contact with graphite is seen to approx. 1% lower transmittance than the reference glass.

The glass that had been in contact with 30 nm film shown an oscillating profile indicating an instrumental error. The other glasses used in contact tests show the spectra very similar to that of the reference one. The second set of measurements can be seen in Figure 4.14.

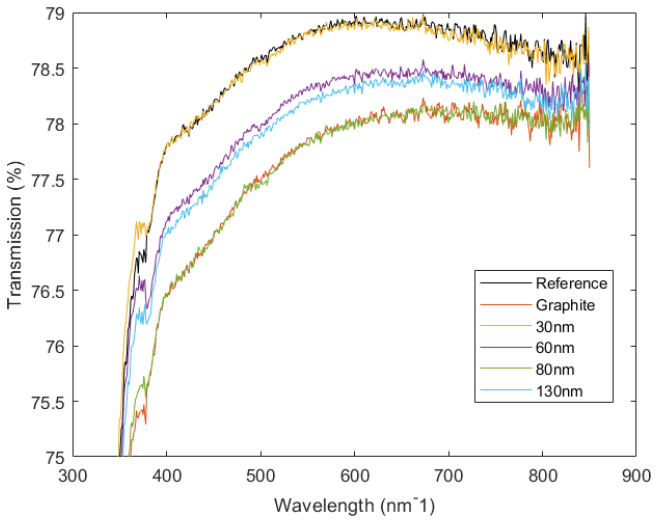

Figure 4.14: Section of the spectrum's done for samples after the contact test

It can be observed that there are three groupings of spectra. The spectrum for the glass being in contact with 30 nm film shows no difference with a reference spectrum. While for the glasses being in contact with thicker films, there is a small decrease in transmittance. Comparing the first and second sets of measurements one can conclude that the glass in contact with graphite shows a stable tendency for decrease of transmission. The graphite sample is seen to be approx.

1 % lower in transmission in both measurement cases. Graphite is expected to oxidize above 400 °C [Mahmood et al., 2019]. Thus, it is likely that some reaction occurred even in the very low oxygen atmosphere used during the contact test, as such a thin layer of graphite oxide could perhaps be formed on the surface of the glass lowering the transmittance.

For the cases of coated samples, there are some changes in intensity, which could be related to a slightly different positioning of the glass into the sample holder. Thus, the 130nm and 80nm transmission are different from the first set of measurements. This could indicate that some nanocrystals had stuck to the glass, but not in a uniform manner.

However, the contact test main focus is to indicate usage. As described in [Klocke et al., 2012] a much more rigorous testing is needed to correctly compare the usage to its real-world counterpart. Especially when considering the influence that glass type used has.

That said the aim of the project is not to develop a new type of coating for industrial purposes but to develop an approach to make a coating that can be used for glass molding applications. Overall the experiments have shown that the coating works as a proof of concept, thus the success criteria are fulfilled.

However, while a successful approach has been created, there are possibilities for further improvements which warrants further investigations.

5 Conclusion

The objective of this project was to develop an approach on the formation of thin thermally stable titanium-based coatings on graphite to be used for glass molds.

PVD was used to deposited titanium film at different thickness unto graphite substrates. The samples were first annealed and then later put into contact with glass pieces at elevated temperatures to evaluate their usage in glass molding applications.

AFM and SEM measurements were used to investigate the morphology and structure of the coatings. It was observed that the graphite surface was very rough and had a "flaky" structure. The as-deposited films were seen to have a nanogranular structure and follow the morphology of the substrate. After annealing a change was observed from a nanogranular structure to a more crystalline structure. Based on comparison with thermal oxidation of titanium films in literature, it was concluded that the film transformation was likely due to a change from titanium to a rutile film. The structural difference between the film deposited onto the silicon and the graphite substrates could perhaps be attributed to a difference in oxidation reaction speed.

EDX data show that trace elements could be found in the substrate, the origin was assigned to the cutting process. A small amount of oxygen was observed in the graphite samples after the contact test, which matched expectations. EDX data for the coated samples found that there was an increase in oxygen content after thermal treatments which indicates oxidation.

Optical spectroscopy was used to see if nanocrystals had stuck to the glass during the contact test. No or very small reduction in transmittance of the glasses in contact with the coated samples was observed indicating no or negligible small sticking to the glass. The graphite samples had indications of interaction due to a consistently lower measured transmission. Thus, the contact test was considered a successful proof of concept.

In summary, an approach for the formation of thin thermally stable titanium-based coatings on graphite was developed and the first series of studies have shown its potential prospects. However, further investigation is needed for the optimization of parameters and technology.

6 Future Investigation

For further development of the approach investigated in the project, a variety of changes and subsequent investigations can be made.

Firstly resolving the technical issues during the sputtering process will help to ensure that the only variance during the deposition is the deposition time.

Making a larger range of thicknesses with the same annealing procedure could help confirm tendencies already seen or perhaps give insight to a tendency that simply did not occur within the given scope e.g. as seen in [Brama et al., 2005] thicker films started flaking when annealed at higher temperatures.

The contact test could be more specifically designed, as mentioned the selection of glass and testing conditions has a large impact on the effectiveness of the coating. Thus, a selection process where glass is investigated for its Tg and chemical composition would be preferable. Testing for different kinds of glass would be useful as well to define the scoop of use for the coating.

Methods such as Raman spectroscopy and XRD could assist in getting better insight into the nature of the crystalline structure.

Furthermore, testing over multiple thermal cycles to gain insight into the degradation of the coating would be advantageous.

Bibliography

Hadiya Ameen and Syed Wilayat, 2019. Hadiya Ameen and Syed Wilayat. In situ synthesis of oxidation and wear resistant coatings on graphite. In *2019 16th International Bhurban Conference on Applied Sciences and Technology (IBCAST)*, pages 92–99. IEEE, 2019.

AS Bakri, MZ Sahdan, F Adriyanto, NA Raship, NDM Said, SA Abdullah and MS Rahim, 2017. AS Bakri, MZ Sahdan, F Adriyanto, NA Raship, NDM Said, SA Abdullah and MS Rahim. Effect of annealing temperature of titanium dioxide thin films on structural and electrical properties. In *AIP Conference Proceedings*, volume 1788, page 030030. AIP Publishing LLC, 2017.

Baptista et al., 2018. Andresa Baptista, Francisco Silva, Jacobo Porteiro, José Míguez and Gustavo Pinto. *Sputtering physical vapour deposition (PVD) coatings: A critical review on process improvement and market trend demands.* Coatings, 8(11), 402, 2018.

Barksdale, 1968. Jelks Barksdale. *The encyclopedia of the chemical elements.* Skokie, Illinois: Reinhold Book Corporation, pages 732–38, 1968.

Bernhardt et al., 2013. F Bernhardt, K Georgiadis, L Dolle, O Dambon and F Klocke. *Development of a ta-C diamond-like carbon (DLC) coating by magnetron sputtering for use in precision glass molding.* Materialwissenschaft und Werkstofftechnik, 44(8), 661–666, 2013.

Kirsten Bobzin, Fritz Klocke, Nazlim Bagcivan, Mara Ewering, Kyriakos Georgiadis and Tobias Münstermann, 2010. Kirsten Bobzin, Fritz Klocke, Nazlim Bagcivan, Mara Ewering, Kyriakos Georgiadis and Tobias Münstermann. Impact behaviour of PtIr-based coatings with different interlayers for glass lens moulding. In *Key Engineering Materials*, volume 438, pages 57–64. Trans Tech Publ, 2010.

Bobzin et al., 2012. Kirsten Bobzin, Nazlim Bagcivan, M Ewering, RH Brugnara and T Münstermann. *Influence of interlayer thickness of a thin noble metal MSIP-PVD coating on compound and system properties for glass lens moulding.* Production Engineering, 6(3), 311–318, 2012.

Bobzin et al., 2014. Kirsten Bobzin, Nazlim Bagcivan, Tobias Brögelmann and Tobias Münstermann. *Correlation between chemical glass components and the glass sticking on sputtered PtIr physical vapour deposition coatings for precision blank moulding.* Materials Sciences & Applications, 5, 316–329, 2014.

Brama et al., 2005. Y.L. Brama, Y. Sun, S.R.K. Dangeti and M. Mujahid. *Response of sputtered titanium films on silicon to thermal oxidation.* Surface and Coatings Technology, 195 (2), 189 – 197, 2005. ISSN 0257-8972.

Brand et al., 2004. J Brand, R Gadow and A Killinger. *Application of diamond-like carbon coatings on steel tools in the production of precision glass components.* Surface and Coatings Technology, 180, 213–217, 2004.

Chang et al., **2017**. Li-Chun Chang, Yu-Zhe Zheng, Yu-Xiang Gao and Yung-I Chen. *Mechanical properties and oxidation resistance of sputtered Cr–W–N coatings.* Surface and Coatings Technology, 320, 196–200, 2017.

Choung Lii Chao, Cheng Bang Huo, Wen Chen Chou, Tzung Shian Wu, Kung Jeng Ma, Chien Huang Kuo, Ying Tung Chen and Chung Woei Chao, 2010. Choung Lii Chao, Cheng Bang Huo, Wen Chen Chou, Tzung Shian Wu, Kung Jeng Ma, Chien Huang Kuo, Ying Tung Chen and Chung Woei Chao. Investigation of the interfacial reaction between optical glasses and various protective films and mold materials. In *Defect and Diffusion Forum*, volume 297, pages 808–813. Trans Tech Publ, 2010.

Choung-Lii Chao, Chia-Jung Chang, Chun-Chieh Chen, Wen-Chen Chou and Kung-Jeng Ma, 2013a. Choung-Lii Chao, Chia-Jung Chang, Chun-Chieh Chen, Wen-Chen Chou and Kung-Jeng Ma. Precision grinding of tungsten carbide mold insert for molding of sub-millimeter glass aspheric lenses. In *International Conference on Optics in Precision Engineering and Nanotechnology (icOPEN2013)*, volume 8769, page 87691U. International Society for Optics and Photonics, 2013a.

Chao et al., **2013b**. Choung-Lii Chao, Cheng-Bang Huo, Wen-Chen Chou, You-Ruei Lin, Kung-Jeng Ma and Hsi-Hsin Chien. *Study on the design of precious metal based protective films for glass moulding process.* Surface and Coatings Technology, 231, 567–572, 2013.

Chaudhry et al., **2018**. AU Chaudhry, Bilal Mansoor, Tarang Mungole, Georges Ayoub and David P Field. *Corrosion mechanism in PVD deposited nano-scale titanium nitride thin film with intercalated titanium for protecting the surface of silicon.* Electrochimica Acta, 264, 69–82, 2018.

Chawla et al., **2009**. Vipin Chawla, R Jayaganthan, AK Chawla and Ramesh Chandra. *Microstructural characterizations of magnetron sputtered Ti films on glass substrate.* journal of materials processing technology, 209(7), 3444–3451, 2009.

Chen and Wang, **2014**. Yung-I Chen and Hsiu-Hui Wang. *Oxidation resistance and mechanical properties of Cr–Ta–Si–N coatings in glass molding processes.* Surface and Coatings Technology, 260, 118–125, 2014.

Chen et al., **2006**. Yung-I Chen, Kuan-Ting Liu, Fan-Bean Wu and Jenq-Gong Duh. *Mo–Ru coatings on tungsten carbide by direct current magnetron sputtering.* Thin solid films, 515(4), 2207–2212, 2006.

Chen et al., **2014**. Yung-I Chen, Kun-Yi Lin, Hsiu-Hui Wang and Kuo-Cheng Lin. *Thermal stability of TaN, CrTaN, TaSiN, and CrTaSiN hard coatings in oxygen-containing atmospheres.* Surface and Coatings Technology, 259, 159 – 166, 2014. ISSN 0257-8972. TACT 2013 International Thin Films Conference.

Chen et al., **2015a**. Yung-I Chen, Yu-Ru Cheng, Li-Chun Chang and Jyh-Wei Lee. *Chemical inertness of Cr–W–N coatings in glass molding.* Thin Solid Films, 593, 102–109, 2015.

Chen et al., 2015b. Yung-I Chen, Yu-Ru Cheng, Li-Chun Chang and Tso-Shen Lu. *Chemical inertness of Ta–Si–N coatings in glass molding.* Thin Solid Films, 584, 66–71, 2015.

Chen et al., 2017. Yung-I Chen, Tso-Shen Lu and Zhi-Ting Zheng. *Internally oxidized Ru-Zr multilayer coatings.* Coatings, 7(4), 46, 2017.

His Hsin Chien, Kung Jeng Ma, Chien Huang Kuo, Cheng Bang Huo, Choung Lii Chao and Ying Tung Chen, 2010. His Hsin Chien, Kung Jeng Ma, Chien Huang Kuo, Cheng Bang Huo, Choung Lii Chao and Ying Tung Chen. The Effect of TaN Interlayer on the Performance of Pt-Ir Protective Coatings in Glass Molding Process. In *Defect and Diffusion Forum*, volume 297, pages 869–874. Trans Tech Publ, 2010.

Dahotre et al., 2001. Narendra B Dahotre, Puja Kadolkar and Swapnil Shah. *Refractory ceramic coatings: processes, systems and wettability/adhesion.* Surface and Interface Analysis: An International Journal devoted to the development and application of techniques for the analysis of surfaces, interfaces and thin films, 31(7), 659–672, 2001.

Dai et al., 1999. Z Dai, H Naramoto, K Narumi and S Yamaoto. *Epitaxial growth of rutile films on Si (100) substrates by thermal oxidation of evaporated titanium films in argon flux.* Journal of Physics: Condensed Matter, 11(43), 8511, 1999.

Devia et al., 2011. DM Devia, E Restrepo-Parra and PJ Arango. *Comparative study of titanium carbide and nitride coatings grown by cathodic vacuum arc technique.* Applied surface science, 258(3), 1164–1174, 2011.

Diebold, 2003. Ulrike Diebold. *The surface science of titanium dioxide.* Surface science reports, 48(5-8), 53–229, 2003.

Dobrzanski et al., 2010. LA Dobrzanski, M Staszuk, K Golombek, A Sliwa and M Pancielejko. *Structure and properties PVD and CVD coatings deposited onto edges of sintered cutting tools.* Archives of Metallurgy and Materials, 55(1), 187–193, 2010.

Dukwen et al. J Dukwen, K Georgiadis, D Hollstegge, D Wachter, O Dambon and F Klocke. *Investigations on the tool wear in precision glass molding.*

Einollahzadeh-Samadi and Dariani, 2013. M Einollahzadeh-Samadi and RS Dariani. *Effect of substrate temperature and deposition rate on the morphology and optical properties of Ti films.* Applied surface science, 280, 263–267, 2013.

Erck and Maiya, 1998. RA Erck and PS Maiya. *Fracture behavior of graphite coated with titanium compounds by chemical vapor deposition.* Materials Science and Engineering: A, 251 (1-2), 251–254, 1998.

Fogarassy et al., 2018. Zsolt Fogarassy, Nikolett Oláh, Ildikó Cora, Zsolt Endre Horváth, Tamás Csanádi, Attila Sulyok and Katalin Balázsi. *The structural and mechanical characterization of TiC and TiC/Ti thin films grown by DC magnetron sputtering.* Journal of the European Ceramic Society, 38(7), 2886–2892, 2018.

Friedrichs et al., **2020**. Marcel Friedrichs, Zirong Peng, Tim Grunwald, Michael Rohwerder, Baptiste Gault and Thomas Bergs. *PtIr protective coating system for precision glass molding tools: Design, evaluation and mechanism of degradation.* Surface and Coatings Technology, 385, 125378, 2020.

Elena Fuentes, Sofia Alves, Ainara López-Ortega, Lucía Mendizabal and Virginia Sáenz de Viteri. Advanced Surface Treatments on Titanium and Titanium Alloys Focused on Electrochemical and Physical Technologies for Biomedical Applications. In *Biomaterial-supported Tissue Reconstruction or Regeneration.* IntechOpen, 2019.

Giannuzzi et al., **2004**. Lucille A Giannuzzi et al. *Introduction to focused ion beams: instrumentation, theory, techniques and practice.* Springer Science & Business Media, 2004.

Greenwood and Earnshaw, **2012**. Norman Neill Greenwood and Alan Earnshaw. *Chemistry of the Elements.* Elsevier, 2012.

Holt and Munir, **1986**. JB Holt and ZA Munir. *Combustion synthesis of titanium carbide: theory and experiment.* Journal of Materials Science, 21(1), 251–259, 1986.

Hong, **2017**. Wonbin Hong. *Solving the 5G mobile antenna puzzle: Assessing future directions for the 5G mobile antenna paradigm shift.* IEEE Microwave Magazine, 18(7), 86–102, 2017.

Hou et al., **2003**. Ya-Qi Hou, Da-Ming Zhuang, Gong Zhang, Ming Zhao and Min-Sheng Wu. *Influence of annealing temperature on the properties of titanium oxide thin film.* Applied Surface Science, 218(1), 98 – 106, 2003. ISSN 0169-4332.

Huang et al., **2007**. Jia-Hong Huang, Fan-Yi Ouyang and Ge-Ping Yu. *Effect of film thickness and Ti interlayer on the structure and properties of nanocrystalline TiN thin films on AISI D2 steel.* Surface and Coatings Technology, 201(16-17), 7043–7053, 2007.

Jin et al., **2009**. Yongzhong Jin, Wei Wu, Li Li, Jian Chen, Jingyu Zhang, Youbing Zuo and Jun Fu. *Effect of sputtering power on surface topography of dc magnetron sputtered Ti thin films observed by AFM.* Applied Surface Science, 255(8), 4673–4679, 2009.

Kaipoldayev et al., **2017**. OE Kaipoldayev, AD Muradov, YS Mukhametkarimov, RR Nemkayeva, GA Baigarinova, MB Aitzhanov and NR Guseinov. *Titanium Carbide Obtained by Magnetron Sputtering of Graphite on Heated Titanium Substrate.* 2017.

Hyun Uk Kim, Sang Hwa Jeong, Hye Jeong Kim and Jeong Ho Kim, 2007. Hyun Uk Kim, Sang Hwa Jeong, Hye Jeong Kim and Jeong Ho Kim. Optical properties of aspheric glass lens using DLC coating mold. In *Key Engineering Materials*, volume 345, pages 1577–1580. Trans Tech Publ, 2007.

Klocke et al., **2011**. F Klocke, K-D Bouzakis, K Georgiadis, S Gerardis, G Skordaris and M Pappa. *Adhesive interlayers' effect on the entire structure strength of glass molding tools' Pt–Ir coatings by nano-tests determined.* Surface and Coatings Technology, 206(7), 1867–1872, 2011.

Fritz Klocke, Olaf Dambon and Kyriakos Georgiadis, 2010. Fritz Klocke, Olaf Dambon and Kyriakos Georgiadis. Comparison of nitride and noble metal coatings for precision glass molding tools. In *Key Engineering Materials*, volume 438, pages 9–16. Trans Tech Publ, 2010.

Klocke et al., 2012. Fritz Klocke, Kyriakos Georgiadis, Olaf Dambon, Konstantinos-Dionysios Bouzakis, Stefanos Gerardis and Georgios Skordaris. *Complete qualification methodology for coatings of precision glass molding tools.* Optical Engineering, 51(7), 073401, 2012.

Klocke et al., 2016. Fritz Klocke, Olaf Dambon, Michael Rohwerder, Frank Bernhardt, Marcel Friedrichs and Sergiy V Merzlikin. *Model of coating wear degradation in precision glass molding.* The International Journal of Advanced Manufacturing Technology, 87(1-4), 43–49, 2016.

Kumar et al., 2017. D Dinesh Kumar, N Kumar, S Kalaiselvam, R Radhika, Arul Maximus Rabel and R Jayavel. *Tribo-mechanical properties of reactive magnetron sputtered transition metal carbide coatings.* Tribology International, 114, 234–244, 2017.

Lee et al., 2018. Seon-Hong Lee, In-Hwan Ko and Tae-Young Kim. *Surface failure analysis of AlCrN coating on WC substrate subjected to high-temperature oxidation in glass-molding machine.* Applied Surface Science, 452, 210–216, 2018.

Liu et al., 2007. Chenglong Liu, Paul K Chu, Guoqiang Lin and Dazhi Yang. *Effects of Ti/TiN multilayer on corrosion resistance of nickel–titanium orthodontic brackets in artificial saliva.* Corrosion Science, 49(10), 3783–3796, 2007.

Liu et al., 2014. Shih-Chang Liu, Yung-I Chen, Jiin-Jyh Shyu, Hung-Yin Tsai, Kun-Yi Lin, Yung-Hsing Chen and Kuo-Cheng Lin. *The chemical inertness of Ir–Re and Ta–Ru coatings in molding B2O3–ZnO–La2O3-based glass.* Surface and Coatings Technology, 259, 352–357, 2014.

Liu et al., 2016. WD Liu, M Liu and LC Zhang. *Oxidation-induced mechanical deterioration and hierarchical cracks in glassy carbon.* Carbon, 100, 178–186, 2016.

Kung Jeng Ma, HH Chien, WH Chuan, Choung Lii Chao and KC Hwang, 2008. Kung Jeng Ma, HH Chien, WH Chuan, Choung Lii Chao and KC Hwang. Design of protective coatings for glass lens molding. In *Key Engineering Materials*, volume 364, pages 655–661. Trans Tech Publ, 2008.

Maehara and Murakoshi, 2002. Hiroyuki Maehara and Hiroshi Murakoshi. *Quartz Glass Molding by Precision Glass Molding Method.* IEEJ Transactions on Sensors and Micromachines, 122, 494–497, 2002.

Menahil Mahmood, Hadiya Ameen, Muhammad Farooq Zafar and Syed Wilayat Husain, 2019. Menahil Mahmood, Hadiya Ameen, Muhammad Farooq Zafar and Syed Wilayat Husain. Development and Characterization of Oxidation Resistant TiC Coating on Graphite. In *2019 16th International Bhurban Conference on Applied Sciences and Technology (IBCAST)*, pages 30–34. IEEE, 2019.

Marin et al., **2016**. E. Marin, R. Offoiach, M. Regis, S. Fusi, A. Lanzutti and L. Fedrizzi. *Diffusive thermal treatments combined with PVD coatings for tribological protection of titanium alloys.* Materials and Design, 89, 314 – 322, 2016. ISSN 0264-1275.

Matthes et al., **1991**. Bernd Matthes, Erhard Broszeit, Jari Aromaa, Helena Ronkainen, S-P Hannula, Adrian Leyland and Allan Matthews. *Corrosion performance of some titanium-based hard coatings.* Surface and Coatings Technology, 49(1-3), 489–495, 1991.

K-O Min, Shuji Tanaka and M Esashi, 2015. K-O Min, Shuji Tanaka and M Esashi. Micro/nano glass press molding using silicon carbide molds fabricated by silicon lost molding. In *18th IEEE International Conference on Micro Electro Mechanical Systems, 2005. MEMS 2005.*, pages 475–478. IEEE, 2015.

Mitterer, **2014**. Christian Mitterer. *PVD and CVD hard coatings.* 2014.

Nicklow et al., **1972**. R Nicklow, N Wakabayashi and HG Smith. *Lattice dynamics of pyrolytic graphite.* Physical Review B, 5(12), 4951, 1972.

NIST. NIST NIST. *Reference on Constants, Units and Uncertainty.*

Nunes et al., **2017**. V. Nunes, F.J.G. Silva, M.F. Andrade, R. Alexandre and A.P.M. Baptista. *Increasing the lifespan of high-pressure die cast molds subjected to severe wear.* Surface and Coatings Technology, 332, 319 – 331, 2017.

Park and Kim, **2002**. In-Wook Park and Kwang Ho Kim. *Coating materials of TiN, Ti–Al–N, and Ti–Si–N by plasma-enhanced chemical vapor deposition for mechanical applications.* Journal of materials processing technology, 130, 254–259, 2002.

Park and Won, **2010**. Soon-Sub Park and Jong-Ho Won. *A Research on DLC Thin Film Coating of a SiC Core for Aspheric Glass Lens Molding.* Journal of the Korean Society for Precision Engineering, 27(12), 28–32, 2010.

Peng et al., **2017**. Zirong Peng, Michael Rohwerder, Pyuck-Pa Choi, Baptiste Gault, Thorsten Meiners, Marcel Friedrichs, Holger Kreilkamp, Fritz Klocke and Dierk Raabe. *Atomic diffusion induced degradation in bimetallic layer coated cemented tungsten carbide.* Corrosion Science, 120, 1–13, 2017.

Poon et al., **2005**. Ray WY Poon, Joan PY Ho, Xuanyong Liu, CY Chung, Paul K Chu, Kelvin WK Yeung, William W Lu and Kenneth MC Cheung. *Formation of titanium nitride barrier layer in nickel–titanium shape memory alloys by nitrogen plasma immersion ion implantation for better corrosion resistance.* Thin solid films, 488(1-2), 20–25, 2005.

Rajput et al., **2018**. Deepak Rajput, Lino Costa, Kathleen Lansford, George M Murray and WilliamH Hofmeister. *Laser-Assisted Deposition of Transition Metal Coatings on Graphite.* Reviews on Advanced Materials Science, 57(2), 158–166, 2018.

Scoggins and Sheppard, **March 14 2019**. Troy Scoggins and Rex Gerald Sheppard. *Coatings for glass shaping molds and molds comprising the same*, 2019. US Patent App. 15/743,080.

Sharif and Rahim, **2007**. S. Sharif and E.A. Rahim. *Performance of coated- and uncoated-carbide tools when drilling titanium alloy—Ti–6Al4V*. Journal of Materials Processing Technology, 185(1), 72 – 76, 2007.

Feng Shi. Introductory Chapter: Basic Theory of Magnetron Sputtering. In *Magnetron Sputtering*. IntechOpen, 2018.

Gaylord D. Smith. Corrosion of Precious Metals and Alloys. In *Corrosion: Materials*. ASM International, 01 2005. ISBN 978-1-62708-183-2.

Suni et al., **1983**. I. Suni, M.-A. Nicolet, C.S. Pai and S.S. Lau. *Stability of amorphous Fe-W alloys in multilayer metallizations on silicon*. Thin Solid Films, 107(1), 73 – 80, 1983.

Ting et al., **2002**. Chu-Chi Ting, San-Yuan Chen and Dean-Mo Liu. *Preferential growth of thin rutile TiO2 films upon thermal oxidation of sputtered Ti films*. Thin Solid Films, 402(1), 290 – 295, 2002. ISSN 0040-6090.

Tseng et al., **2011**. Shih-Feng Tseng, Chao-Te Lee, Kuo-Cheng Huang, Donyau Chiang, Chien-Yao Huang and Chang-Pin Chou. *Mechanical properties of Pt-Ir and Ni-Ir binary alloys for glass-molding dies coating*. Journal of nanoscience and nanotechnology, 11(10), 8682–8688, 2011.

Wang et al., **2015**. Li Wang, Wei-Guo Jiang, Xiang-Wei Li, Jia-Sheng Dong, Wei Zheng, Hui Feng and Lang-Hong Lou. *Effect of surface roughness on the oxidation behavior of a directionally solidified Ni-based superalloy at 1,100 C*. Acta Metallurgica Sinica (English Letters), 28(3), 381–385, 2015.

Zhibin Wang, Mingyin Jiao, Yunlong Zhang, Feng Zhang and Zhongqiang Wang, *2019*. Zhibin Wang, Mingyin Jiao, Yunlong Zhang, Feng Zhang and Zhongqiang Wang. Selection of coating for low Tg glass precision glass molding. In *9th International Symposium on Advanced Optical Manufacturing and Testing Technologies: Advanced Optical Manufacturing Technologies*, volume 10838, page 108381U. International Society for Optics and Photonics, 2019.

Wei et al., **2019**. Junjun Wei, Xiaoyan Zhu, Liangxian Chen, Jinlong Liu and Chengming Li. *High quality anti-sticking coating based on multilayer structure*. Surface and Coatings Technology, 362, 72–77, 2019.

Wood, **1962**. RM Wood. *The lattice constants of high purity alpha titanium*. Proceedings of the Physical Society, 80(3), 783, 1962.

Xie et al., **2011**. ZW Xie, LP Wang, XF Wang, L Huang, Y Lu and JC Yan. *Influence of high temperature annealing on the structure, hardness and tribological properties of diamond-like carbon and TiAlSiCN nanocomposite coatings*. Applied surface science, 258(3), 1206–1211, 2011.

Yan et al., **2019**. Hongjuan Yan, Qinye Tian, Dewen Gao and Feifei Yang. *Microstructure and properties of TiAlN/AlN multilayers with different modulation periods*. Surface and Coatings Technology, 363, 61–65, 2019.

Yang et al., **2017**. Jin-hua Yang, Quan-gui Guo, Zhan-jun Liu, Hai-peng Qiu and Jian Jiao. *The structure of an in-situ formed titanium-boron-carbon coating on a graphite substrate.* New Carbon Materials, 32(5), 474–480, 2017.

Yildiz et al., **2009**. Fahrettin Yildiz, AF Yetim, Akgün Alsaran and I Efeoglu. *Wear and corrosion behaviour of various surface treated medical grade titanium alloy in bio-simulated environment.* Wear, 267(5-8), 695–701, 2009.

Yin et al., **2005**. Xiaowei Yin, I Gotman, L Klinger and EY Gutmanas. *Formation of titanium carbide on graphite via powder immersion reaction assisted coating.* Materials Science and Engineering: A, 396(1-2), 107–114, 2005.

Gorkem Yumusak. Evaluating the Effect of Titanium-Based PVD Metallic Thin Films on Nitrogen Diffusion Efficiency in Duplex Plasma Diffusion/Coating Systems. PhD thesis, University of Sheffield, 2019.

Hongbin Zang, Jiaxin Yu, Yingyue Zhou and Bo Tao, *2014*. Hongbin Zang, Jiaxin Yu, Yingyue Zhou and Bo Tao. Non-isothermal molding technology research of ultra-precision glass lens. In *International Symposium on Optoelectronic Technology and Application 2014: Laser Materials Processing; and Micro/Nano Technologies*, volume 9295, page 929517. International Society for Optics and Photonics, 2014.

L Zhang, G Liu, X Zhao, Olaf Dambon, F Klocke and AY Yi, *2016*. L Zhang, G Liu, X Zhao, Olaf Dambon, F Klocke and AY Yi. Precision molding of optics: a review of its development and applications. In *Polymer Optics and Molded Glass Optics: Design, Fabrication, and Materials 2016*, volume 9949, page 994906. International Society for Optics and Photonics, 2016.

Zhang and Liu, **2017**. Liangchi Zhang and Weidong Liu. *Precision glass molding: Toward an optimal fabrication of optical lenses.* Frontiers of Mechanical Engineering, 12(1), 3–17, 2017.

Zhang et al., **2020**. Mingming Zhang, Yuxian Cheng, Li Xin, Jianxiu Su, Yongfeng Li, Shenglong Zhu and Fuhui Wang. *Cyclic oxidation behaviour of Ti/TiAlN composite multilayer coatings deposited on titanium alloy.* Corrosion Science, page 108476, 2020. ISSN 0010-938X.

Zhu et al., **2015**. Xiao-yan Zhu, Jun-jun Wei, Liang-xian Chen, Jin-long Liu, Li-fu Hei, Cheng-ming Li and Yong Zhang. *Anti-sticking Re-Ir coating for glass molding process.* Thin Solid Films, 584, 305–309, 2015.

Appendix A

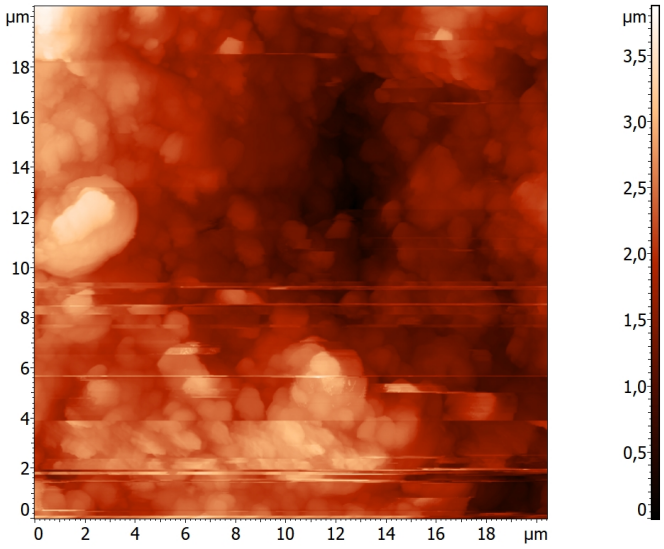

AFM image 1

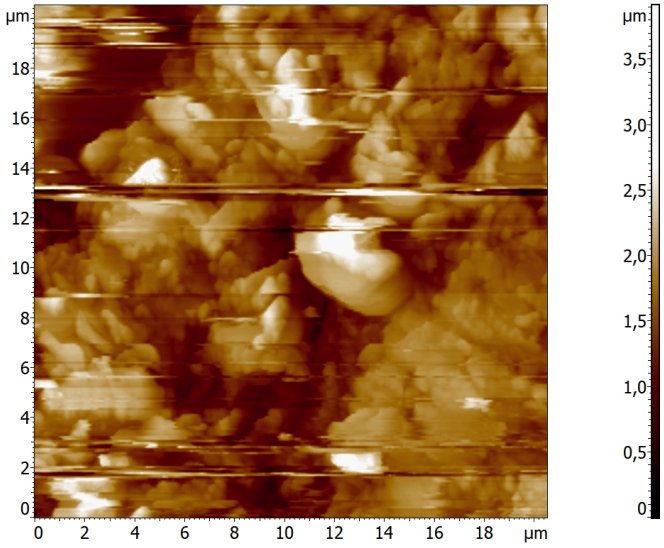

AFM image 3

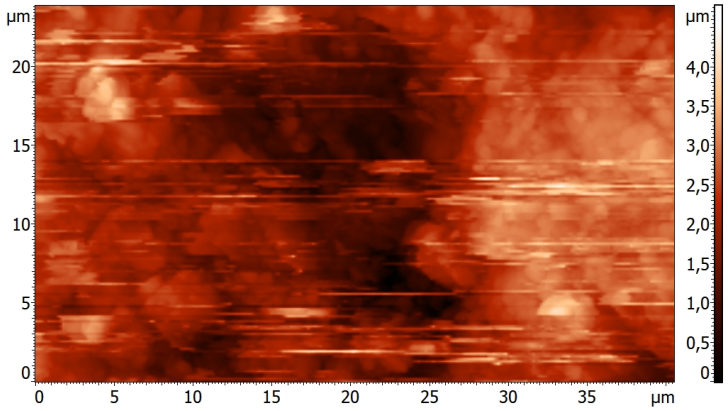

AFM image 4

Appendix B

Atomic % data for 80nm samples as-deposited, annealed and after contact test, respectively

Area/Elements	C-K	N-K	O-K	Na-K	Al-K	Si-K	Cl-K	K-K	Ti-K
80nm pt1	74,36	11,34	6,67	0,6	0,06	0	0,53	0,23	6,21
80nm pt2	73,9	8,5	5,82	0,46	0,06	0	0,46	0,19	10,62
80nm pt3	75,25	10,32	6,11	0,69	0	0,07	0,59	0,28	6,69
80nm pt4	76	10,08	5,97	0,48	0,03	0	0,44	0,15	6,84
average ± SD	74,88±0,81	10,06±1,02	6,14±0,32	0,56±0,09	0,04±0,02	0,02±0,03	0,51±0,06	0,21±0,05	7,59±1,76
Area/Elements	C-K	O-K	Al-K	Si-K	S-K	Ca-K	Ti-K	Mo-L	
80anneal pt1	83,27	11,3	0,29	0,06	0,03	0	5,05	0	
80anneal pt2	83,1	11,62	0,24	0,05	0	0	4,99	0	
80anneal pt3	82,79	11,71	0,32	0,08	0	0,04	5,06	0	
80anneal pt4	77,35	15,4	0,43	0,08	0	0	6,71	0,03	
average ± SD	81,63±2,48	12,51±1,68	0,32±0,07	0,07±0,01	0,01±0,01	0,01±0,02	5,45±0,73	0,01±0,01	
Area/Elements	C-K	N-K	O-K	Na-K	Al-K	Si-K	S-K	Ca-K	Ti-K
80contact pt1	75,61	0	16,83	0,08	0,08	0,13	0	0	7,27
80contact pt2	76,1	0	16,91	0,12	0,08	0,11	0	0	6,68
80contact pt3	81,29	0	12,53	0,09	0,08	0,18	0,03	0,1	5,71
80contact pt4	58,87	15,23	18,2	0,11	0,14	0,09	0	0	7,35
average ± SD	72,97±8,44	3,81±6,59	16,12±2,14	0,10±0,02	0,10±0,03	0,13±0,03	0,01±0,01	0,03±0,04	6,75±0,66

Atomic % data for 130nm samples as-deposited, annealed and after contact test, respectively

Area/Elements	C-K	N-K	O-K	Na-K	Al-K	Si-K	Ti-K		
130 pt1	73,91	3,32	9,55	0,04	0,1	0,16	12,91		
130 pt2	73,57	3,76	8,51	0	0,07	0,1	13,99		
130 pt3	75,37	2,74	8,1	0,08	0,06	0	13,65		
130 pt4	74,59	4,14	8,1	0	0,04	0,09	13,04		
average ± SD	74,36±0,80	3,49±0,60	8,57±0,68	0,03±0,04	0,07±0,03	0,09±0,07	13,40±0,51		
Area/Elements	C-K	N-K	O-K	Al-K	Si-K	Ca-K	Ti-K	Cr-K	W-M
130anneal pt1	61,51	0	25,74	0,08	0	0	12,56	0	0,11
130anneal pt2	65,61	0	22,83	0	0	0	11,48	0	0,08
130anneal pt3	81,74	0	12,25	0	0	0	5,95	0	0,06
130anneal pt4	76,71	0	9,9	0	0,17	0,24	12,12	0,81	0,05
average ± SD	71,39±9,42	0,00±0,00	17,68±7,78	0,02±0,04	0,04±0,09	0,06±0,12	10,53±3,08	0,20±0,41	0,08±0,03
Area/Elements	C-K	N-K	O-K	Al-K	Si-K	Ca-K	Ti-K		
130contact pt1	54,31	0	29,11	2,63	0,06	0	13,88		
130contact pt2	67,82	0	20,59	1,81	0,08	0,08	9,62		
130contact pt3	59,17	0	25,6	2,61	0,05	0,08	12,48		
130contact pt4	52,96	0	28,45	2,99	0,13	0	15,47		
average ± SD	58,57±6,72	0,00±0,00	25,94±3,88	2,51±0,50	0,08±0,04	0,04±0,05	12,86±2,48		

Appendix C

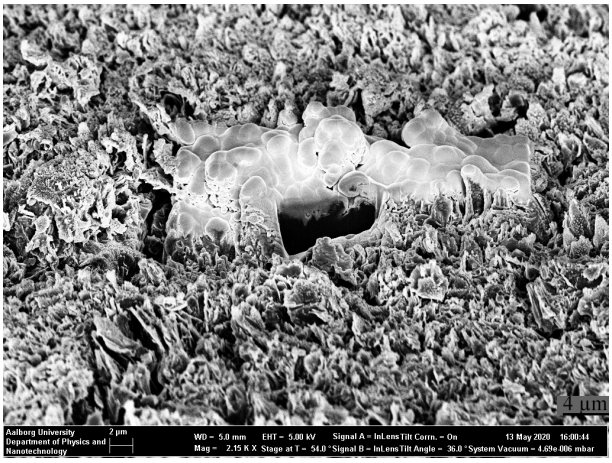

(a)

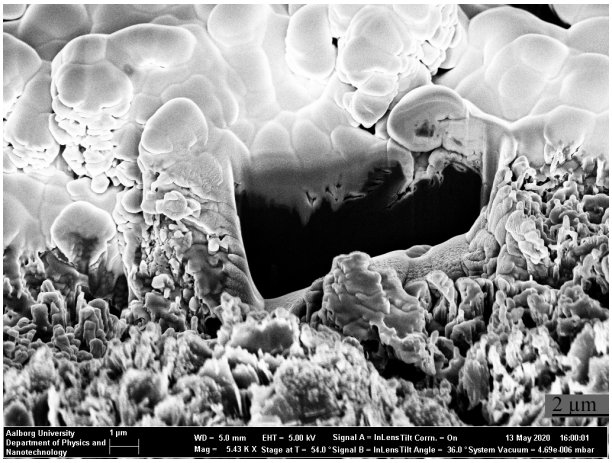

(b)

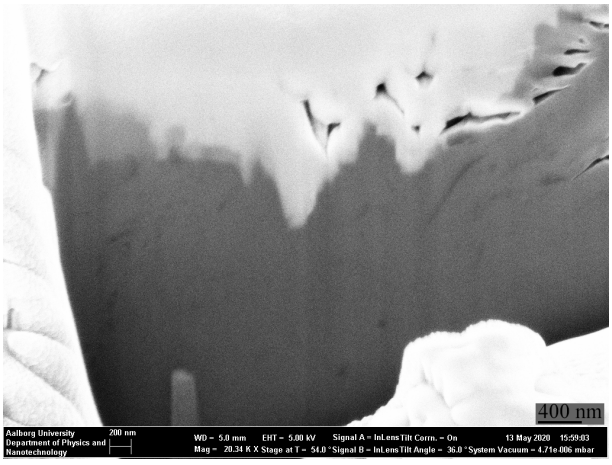

(c)

a) SEM images of FIB cut area with different magnification. The distinct white area is deposition platinum used for area markings. There is no indications of layer formation.

Appendix D

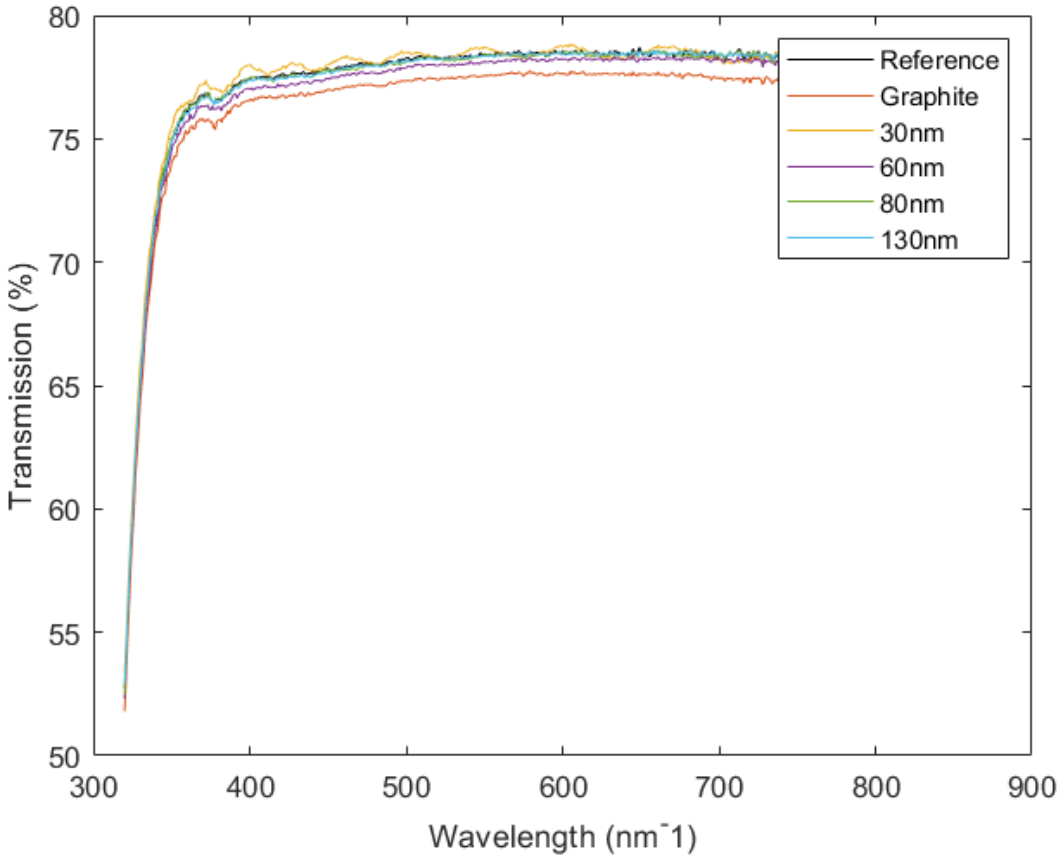

Spectrum's of samples after the contact test, first set of measurements

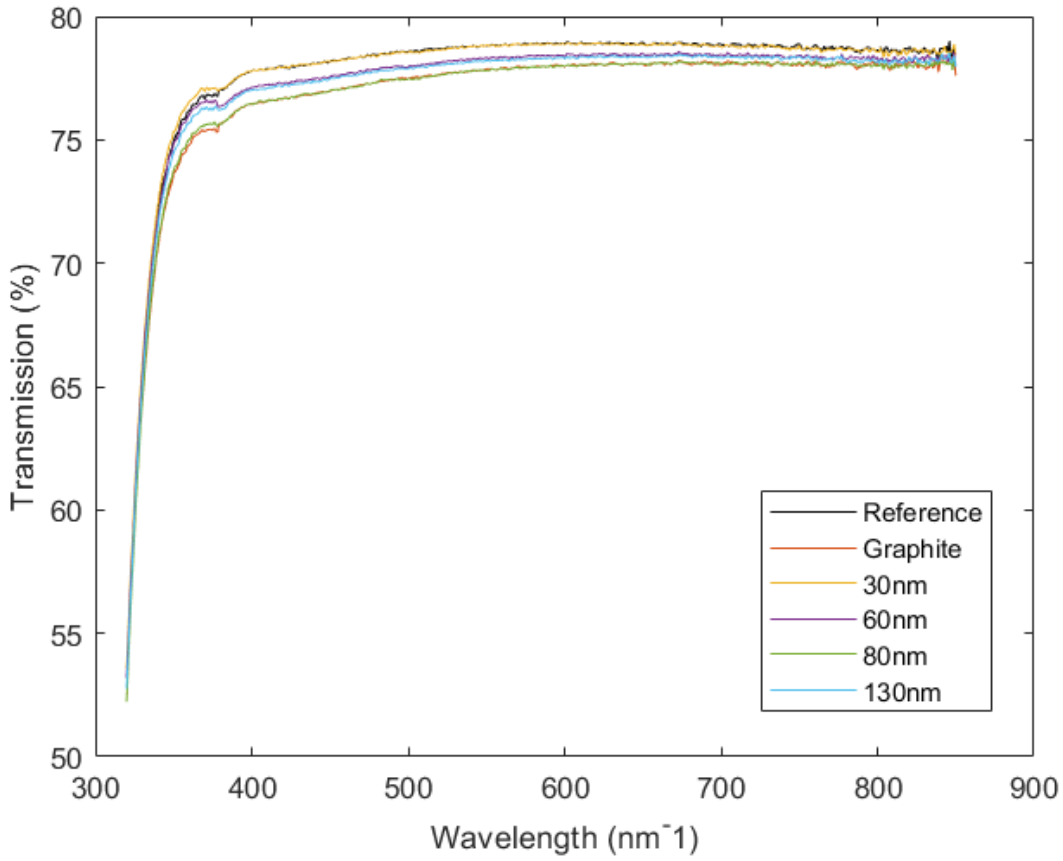

Spectrum's of samples after the contact test, second set of measurements